January 2021

Development Of A Dynamic Force Sensor

Olusola Andrew Bolaniran

DEVELOPMENT OF A DYNAMIC FORCE SENSOR

by

Olusola Andrew Bolaniran
Bachelor of Engineering, Federal University of Technology Akure, 2009

A Thesis
Submitted to the Graduate Faculty

Of the

University of North Dakota
in partial fulfilment of the requirements

for the degree of
Master of Science

Grand Forks, North Dakota

May
2021

This thesis, submitted by Olusola Andrew Bolaniran in partial fulfilment of the requirements for the Degree of Master of Science from the University of North Dakota has been read by the Faculty Advisory Committee under whom the work has been done and is hereby approved.

_____

Dr. Djedje-kossu Zahui (Committee Chair)

_____

Dr. Cai Xia Yang (Committee Member)

_____

Dr. Surojit Gupta (Committee Member)

_____

Dr. Hallie Chelmo (Committee Member)

This thesis is being submitted by the appointed advisory committee as having met all of the requirements of the school of Graduate Studies at the University of North Dakota and is hereby approved.

_____

Chris Nelson

Dean of the School of Graduate Studies

_____

Date

PERMISSION

Title: Development of A Dynamic Force Sensor

Department Mechanical Engineering

Degree Master of Science

In presenting this thesis in partial fulfilment of the requirements for a graduate degree from the University of North Dakota, I agree that the library of this University shall make if freely available for inspection. I further agree that permission for extensive copying for scholarly purposes may be granted by the professor who supervised my thesis work or in his absence, by the Chairperson of the department or the dean of the School of Graduate Studies. It is understood that any copying or publication or other use of this thesis or part thereof for financial gain shall not be allowed without my written permission. It is also understood that due recognition shall be given to me and to the University of North Dakota in any scholarly use which may be made of any material in my thesis.

Olusola Bolaniran

May 2021

Table of Contents

PERMISSION iv

LIST OF FIGURES viii

LIST OF TABLES x

ACKNOWLEDGMENTS xi

ABSTRACT xii

CHAPTER 1 ..... **Error! Bookmark not defined.**

INTRODUCTION 1

1.1 Overview 1
1.2 Piezoelectric behavior of materials 2
1.3 Piezoelectric Materials 4
1.4 Piezoelectricity 5
1.4.1 Coupling factor k 9

CHAPTER TWO ..... **Error! Bookmark not defined.**

LITERATURE REVIEW 11

2.1 Overview 11
2.2 Load magnitude sensing 11
2.3 Energy Harvesting 19
2.3.1 Energy Harvesting using piezoelectricity 19
2.4 Structural health monitoring 21
2.5 Significance of the work 22

CHAPTER THREE ..... **Error! Bookmark not defined.**

THEORETICAL DEVELOPMENT 23

3.1 Overview 23

3.2 Sensor concept and configuration 23
3.3 Volume displacement 25
3.4 Volume Displacement Measurement 26
3.5 Sensor Equations 30
3.5.1 Static Excitation 31
3.5.2 Harmonic Excitation 33
3.7 Sensor Development Assumptions and Limitations 35
CHAPTER FOUR ..... **Error! Bookmark not defined.**

NUMERICAL VALIDATION 36

4.1 Overview 36
4.2 Material Selection 36
4.2.1 Piezoelectric Material Selection 36
4.2.2 Beam Substrate Selection 38
4.3 Finite Element Analysis and Simulation 39
4.3.1 Geometry generation 39
4.3.2 Meshing 40
4.3.3 Boundary Condition and Loading 42
4.3.4 Results 44
The simulation of the response of the sensor to a random excitation is shown in Fig. 4.22 47

4.3.5 Measurement Error 48
CHAPTER FIVE ..... **Error! Bookmark not defined.**

EXPERIMENTAL VALIDATION 49

5.1 Overview 49
5.2 Sensor Fabrication 49
5.3 Experimental Setup 51
5.4 Experimental Run 55
CHAPTER SIX ..... **Error! Bookmark not defined.**

RESULTS AND DISCUSSIONS 57

6.1 Overview 57
6.2 Results 57
6.3 Temperature Change Effect on the Sensor 59
6.4 Sensor Packaging 62
6.5 Contribution 63
6.6 Conclusion 63
6.7 Future Work 64
APPENDICES 65

Appendix A: Post Processing code 66
REFERENCES 70

LIST OF FIGURES

Figure 1.1: An intermingling of electric and elastic phenomena (Dahiya, 2013)..... 3

Figure 1.2: Piezoelectric effect explained with a simple molecular model 3

Figure 1.3: Tensor directions for defining the constitutive relations..... 7

Figure 2.1:A foil strain gage. (Piersol, 2002) 12

Figure 2.2: Main parts of Hydraulic load cell (Instrumentation tools)..... 13

Figure 2.3: A cross section of a pneumatic load cell. (Bela, 2003) 15

Figure 2.4: Capacitance Pressure sensor (Bela, 2003)..... 16

Figure 2.5: A typical piezoelectric sensor (Avnet, 2019) 17

Figure 3.1: Schematic representation of the sensor system 24

Figure 3.2: Configuration of the sensor 25

Figure 3.3: Deflection of the sensor..... 26

Figure 3.4: Beam with a shaped piezoelectric material 27

Figure 3.5: Shaped piezoelectric film for the fixed-fixed boundary condition..... 30

Figure 3.6: Beam deflection under static load 31

Figure 4.1: Points representing the sensor film in ANSYS 40

Figure 4.2: Measured random force and the excitation force 40

Figure 4.3: Film meshing..... 41

Figure 4.4: Sensor substrate meshing 41

Figure 4.5: Completed meshed sensor..... 42

Figure 4.6: Boundary condition and sensor loading 42

Figure 4.7: Simulation force details..... 43

Figure 4.8: Simulation piezoelectric body details..... 43

Figure 4.9: simulated output voltage from the sensor..... 44

Figure 4.10a: Result at 30Hz 45

Figure 4.11: Sensor response to random excitation..... 48

Figure 5.1: Sensor substrate design 49

Figure 5.2: Machined Sensor substrate..... 50

Figure 5.3: Completed Sensor..... 50

Figure 5.4: Dynamic Signal Analyzer 51

Figure 5.5: Signal Amplifier..... 52

Figure 5.6: Shaker Unit..... 52

Figure 5.7: Data Recording Unit..... 53

Figure 5.8: Setup Schematic 54

Figure 5.9: Experimental Setup 55

Figure 6.1: Result at 20Hz..... 57

Figure 6.2: Sensor response to random excitation..... 58

Figure 6.3: Designed sensor package..... 62

Figure 6.4: Designed sensor package..... 63

LIST OF TABLES

Table 4.1: Properties of PVDF film 37

Table 4.2: Dimensions of beam substrate 38

ACKNOWLEDGMENTS

This document shows the record of the work done as part of my Graduate Studies. It's an evidence to the countless number of hours of research, experiment and writing. It would not have been possible without the guidance of my advisor Dr. Djedje-Kossu Zahui who held my hand through all the crossings in my graduate studies career. I am forever grateful. Special appreciation to my committee members Dr. Cai Xia Yang, Dr. Surojit Gupta and Dr. Hallie Chelmo for their invaluable support, suggestions and support. I am indebted to Jay Evenstad for his help and guidance in machining the experimental specimens. I would like to thank everyone at the Mechanical Engineering Department for their assistance during my graduate studies at UND. Finally, I would like to thank all my family and friends for the prayers during this time.

ABSTRACT

Sensors are employed for various applications in different industries. Chief of these applications is in the process and equipment monitoring. Most sensors used in the equipment monitoring are mostly after-market devices. This research answered the question of how can we include the condition monitoring of equipment into the design phase of the equipment. This research developed a dynamic force sensor using a PolyVinyliDene Fluoride (PVDF) film. The piezoelectric film attached to a fixed-fixed substrate which serves to support film and the properties of which the sensor equations were based. The sensor was tested in the laboratory by subjecting it to harmonic and random excitations of different magnitude and frequencies.

The measured force as obtained from the sensor is compared to the corresponding excitation force in plots. The results obtained show that the sensor is accurate with an error of about 7% for an excitation with a frequency lesser than the first natural frequency of the substrate of the sensor. This result shows that dynamic sensors using piezoelectric materials can be designed and adapted to any application with the selection of the right substrate and boundary conditions.

Chapter 1
Introduction

1.1 Overview

The advances in engineering has led to the design and production of life-changing structures and machines. The reliability as well as the safety of these structures and machines are critical. Constant efficient health monitoring of structures has emerged and important in maintaining the reliability of structures. These health monitoring are being done and implemented in several ways; the chief of which is in smart structures. Structural systems are usually termed smart because they are able to sense and compensate their response to the changing operational or environmental conditions. They achieve this feat by the integration of sensors and actuators to the structural system whereby the sensor measures the external influence while the embedded algorithm compensates for these influences using the actuators. Typical sensors for these monitoring are strain gauges, accelerometers, fibre optics and piezoelectric materials.

Piezoelectric materials are among the most widely used when it comes to smart structures because of their simplicity, reliability and sensitivity. By employing the principle of the direct piezoelectric effect, we are able to sense the load variation on structures. These sensing are usually done using the more flexible piezoelectric materials such as the Polyvinylidene fluoride (PVDF) while the stiffer lead zirconate titanate (PZT) transducers can be used as an actuator for compensation purposes.

The study made in this research focuses on the development of load sensors by applying the piezoelectric principle and the material of choice is PVDF. PVDF is a favored material for designing miniature sensing application and this study investigates application of the material to the development of dynamic sensor.

The phenomenon whereby piezoelectric materials temporarily produce charges when subjected to mechanical stress makes it suitable to quantify an applied load without external energy. This research focuses on the use of a piezoelectric material in this case PVDF to develop a dynamic sensor that can be used to quantify the loading on a structure. This research uses experimental approach as well as analytical techniques to develop and optimize the dynamic sensor.

The documentation of this study presented here is done in five chapters. Chapter 1 outlines the objectives, motivation, the materials and the general equations that are important for our study.

Chapter 2 gives detailed account of literatures on the study of piezoelectricity as applicable to the measurement of variable loading. It discusses the advances in the development of dynamic load sensors.

Chapter 3 documents and discusses the simulation method used to develop and validate the dynamic sensor. It shows all the simulation models created and employed.

Chapter 5 presents the results from the simulation and experiments. Also discussions based on these results are made to draw conclusion from this research.

1.2 Piezoelectric behavior of materials

Piezoelectric materials are class of dielectric materials which can be polarized by an electric field as well as a mechanical stress which is termed the piezoelectric effect.

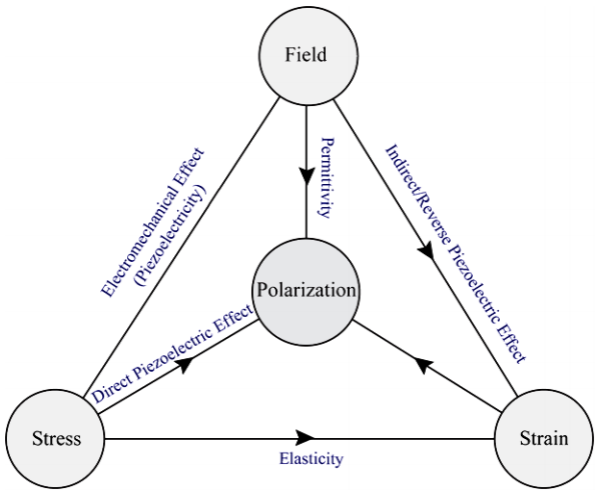

Figure 1.1: An intermingling of electric and elastic phenomena (Dahiya, 2013)

Before the material is subjected to an external stress, the centers of the negative and the positive charges of each molecule coincide resulting into an electrically neutral molecule as depicted in figure below

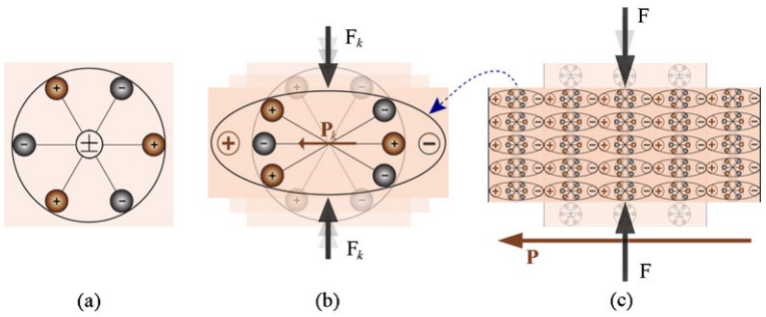

Figure 1.2: Piezoelectric effect explained with a simple molecular model

Upon the application of an external mechanical stress, the internal reticular is deformed thus causing the separation of the positive and negative centers of the molecule and generating little

dipole as depicted in Fig. 1.2b. This causes the opposite facing poles inside the material cancel each other and fixed charges appear on the surface as Fig. 1.2c depicted.

1.3 Piezoelectric Materials

Piezoelectric materials are mostly polymers and ceramics. The largest structure type of piezoelectric ceramics is the perovskite family which consists of mixed oxides of oxygen ions [19] and few of the ceramics are lithium niobate ($LiNbO_3$), lithium tantalite ($LiTaO_3$), barium titanate ($BaTiO_3$), lead titanate ($PbTiO_3$). Common in the piezoelectric ceramic family is the PZT, a binary solution of lead zirconate (PZ, an antiferroelectric) and lead titanate (PT, a ferroelectric). PZT is brittle and have a low tensile strength which limits their application therefore putting emphasis on piezoelectric polymers to be used in sensor applications.

Quartz (SiO_2) is a ceramic that was first commercial exploited as a piezoelectric material. It has high permissible surface pressure of about 150 N/mm2, can withstand temperatures up to 500 OC, very high rigidity, high linearity and negligible hysteresis, constant sensitivity over a wide temperature range which all make Quartz an excellent piezoelectric material.

Zinc Oxide is a relatively soft piezoelectric material which has been used in MEMs as surface wave (WAS) or bulk acoustic wave (BAW) resonators. The pressure-sensing ability was investigated by Kuoni et al [20]. They studied the ZnO thin film that were placed in different positions of flow chamber to measure the liquid pressure difference, thus indicating the flow speed.

PVDF is a polymer that has become appealing to many industries due to its striking characteristics. They are inexpensive, lightweight, biologically compatible, mechanically stable structures and have high electromechanical coefficients which make them suitable as a piezoelectric sensor. They can undergo significant amount of deformation under mechanical stress.

PVDF and PZT both have their advantages and disadvantages. To optimize the performance of a piezoelectric material, the combined properties of ceramic and polymer is considered. Composites are multiphase materials which show the properties of both ceramic and polymers. They are composed of two phases: Matrix phase and dispersed or discrete phase. Dispersed phase refers to the distribution of particles of one constituent and matrix phase surrounds the dispersed phase to make a continuous medium.

1.4 Piezoelectricity

The ability of a material to give out electrical charge under mechanical deformation is known as piezoelectricity. The term "piezo" derives from the Greek meaning "to press" [1]. The phenomenon was discovered by the Curie brothers in 1880 who found that materials like topaz and quartz were accompanied by macroscopic polarization which produces the electric surface charges [2]. A year later, Lippmann [3], predicted converse effect of generating mechanical deformations or strains by imposing voltage on the material.

Based on the linear theory of piezoelectricity, piezoelectric materials operations are restricted to the linear range at low electric fields and at low mechanical stress. Following this theory, the density of the generated fixed charge in a piezoelectric material is proportional to the external stress.

$$P_{pe} = d \times T \tag{1-1}$$

where P_{pe} is the piezoelectric polarization vector whose magnitude is equal to the fixed charge density produced, d is the piezoelectric strain coefficient and T is the stress to which the material is subjected.

Conversely, the reverse piezoelectric effect can be formulated as

$$S_{pe} = d \times E \tag{1-2}$$

where S_{pe} is the mechanical strain produced and E the magnitude of the applied electric field

If we consider the elastic properties of the material, equations (1-1) becomes

$$P_{pe} = d \times T = d \times c \times S = e \times S \tag{1-3}$$

while equation (1-2) becomes

$$T_{pe} = c \times S_{pe} = c \times d \times E = e \times E \tag{1-4}$$

where c is the elastic constant relating to the generated stress, s is the compliance coefficient which relates the deformation to the stress and e is the piezoelectric stress constant.

The piezoelectricity is a cross coupling between the elastic variables, stress T and Strain S, and the dielectric variables, electric charge density D and electric field E. The tensor relation to identify this coupling is given as:

$$S_p = s_{pq}^{E} T_q + d_{pk} E_k \tag{1-5}$$

$$D_i = d_{iq}T_q + \varepsilon_{ik}^T E_k \tag{1-6}$$

where s_{pg}^E is elastic compliance tensor at constant electric field, ε_{ik}^T is dielectric constant tensor under constant stress, d_{kp} is piezoelectric constant tensor, S_p is the mechanical strain in p direction, D_i is electric displacement in $\underline{i}$ direction, T_q is mechanical stress in q direction, and E_k is the electric field in the k direction.

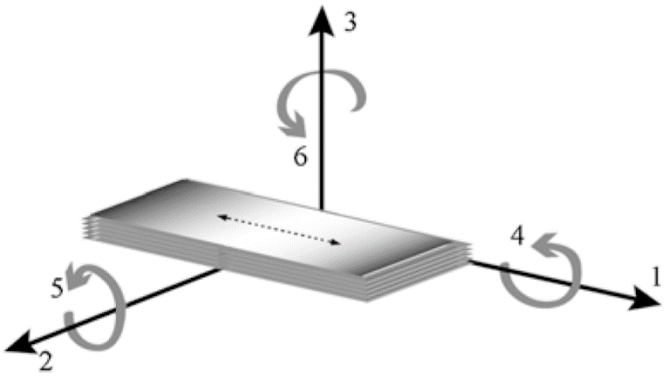

Figure 1.3: Tensor directions for defining the constitutive relations

As the tensor direction illustrated in Fig. 1.3 for piezoelectric materials such as PVDF, the stretch direction is denoted as "1" and the axis orthogonal to the stretch direction in the plane of the film becomes "2". The polarization axis (perpendicular to the surface of the film) is denoted as "3". The shear planes are indicated by the subscripts "4", "5", "6" and are perpendicular to the directions "1", "2" and "3" respectively. Applying this directions, Eqn. (1-5) and (1-6) can be written as

$$\begin{bmatrix} S_1 \\ S_2 \\ S_3 \\ S_4 \\ S_5 \\ S_6 \end{bmatrix} = \begin{bmatrix} s_{11}^E & s_{12}^E & s_{13}^E & s_{14}^E & s_{15}^E & s_{16}^E \\ s_{21}^E & s_{22}^E & s_{23}^E & s_{24}^E & s_{25}^E & s_{26}^E \\ s_{31}^E & s_{32}^E & s_{33}^E & s_{34}^E & s_{35}^E & s_{36}^E \\ s_{41}^E & s_{42}^E & s_{43}^E & s_{44}^E & s_{45}^E & s_{46}^E \\ s_{51}^E & s_{52}^E & s_{53}^E & s_{54}^E & s_{55}^E & s_{56}^E \\ s_{61}^E & s_{62}^E & s_{63}^E & s_{64}^E & s_{65}^E & s_{66}^E \end{bmatrix} \begin{bmatrix} T_1 \\ T_2 \\ T_3 \\ T_4 \\ T_5 \\ T_6 \end{bmatrix} + \begin{bmatrix} d_{11} & d_{12} & d_{13} \\ d_{21} & d_{22} & d_{23} \\ d_{31} & d_{32} & d_{33} \\ d_{41} & d_{42} & d_{43} \\ d_{51} & d_{52} & d_{53} \\ d_{61} & d_{62} & d_{63} \end{bmatrix} \begin{bmatrix} E_1 \\ E_2 \\ E_3 \end{bmatrix} \quad (1\text{-}7)$$

$$\begin{bmatrix} D_1 \\ D_2 \\ D_3 \end{bmatrix} = \begin{bmatrix} d_{11} & d_{12} & d_{13} & d_{14} & d_{15} & d_{16} \\ d_{21} & d_{22} & d_{23} & d_{24} & d_{25} & d_{26} \\ d_{31} & d_{32} & d_{33} & d_{34} & d_{35} & d_{36} \end{bmatrix} \begin{bmatrix} T_1 \\ T_2 \\ T_3 \\ T_4 \\ T_5 \\ T_6 \end{bmatrix} + \begin{bmatrix} \varepsilon_{11}^T & \varepsilon_{12}^T & \varepsilon_{13}^T \\ \varepsilon_{12}^T & \varepsilon_{22}^T & \varepsilon_{23}^T \\ \varepsilon_{31}^T & \varepsilon_{32}^T & \varepsilon_{33}^T \end{bmatrix} \begin{bmatrix} E_1 \\ E_2 \\ E_3 \end{bmatrix} \quad (1\text{-}8)$$

It is observed that the piezoelectric coefficients, d_{ij} for the mechanical and the electrical responses are identical giving opportunity to develop the global response by a matrix that couple both the electrical and mechanical behaviors as written here

$$\begin{Bmatrix} S_1 \\ S_2 \\ S_3 \\ S_4 \\ S_5 \\ S_6 \\ D_1 \\ D_2 \\ D_3 \end{Bmatrix} = \begin{bmatrix} S_{11}^{ET} & S_{12}^{ET} & S_{13}^{ET} & S_{14}^{ET} & S_{15}^{ET} & S_{16}^{ET} & d_{11}^{T\theta} & d_{12}^{T\theta} & d_{13}^{T\theta} \\ S_{21}^{ET} & S_{22}^{ET} & S_{23}^{ET} & S_{24}^{ET} & S_{25}^{ET} & S_{26}^{ET} & d_{22}^{T\theta} & d_{22}^{T\theta} & d_{23}^{T\theta} \\ S_{31}^{ET} & S_{32}^{ET} & S_{33}^{ET} & S_{34}^{ET} & S_{35}^{ET} & S_{36}^{ET} & d_{31}^{T\theta} & d_{32}^{T\theta} & d_{33}^{T\theta} \\ S_{41}^{ET} & S_{42}^{ET} & S_{43}^{ET} & S_{44}^{ET} & S_{45}^{ET} & S_{46}^{ET} & d_{41}^{T\theta} & d_{42}^{T\theta} & d_{43}^{T\theta} \\ S_{51}^{ET} & S_{52}^{ET} & S_{53}^{ET} & S_{54}^{ET} & S_{55}^{ET} & S_{56}^{ET} & d_{51}^{T\theta} & d_{52}^{T\theta} & d_{53}^{T\theta} \\ S_{61}^{ET} & S_{62}^{ET} & S_{63}^{ET} & S_{64}^{ET} & S_{65}^{ET} & S_{66}^{ET} & d_{61}^{T\theta} & d_{62}^{T\theta} & d_{63}^{T\theta} \\ d_{11}^{E.T} & d_{12}^{E.T} & d_{13}^{E.T} & d_{14}^{E.T} & d_{15}^{E.T} & d_{16}^{E.T} & \varepsilon_{11}^T & \varepsilon_{12}^T & \varepsilon_{13}^T \\ d_{21}^{E.T} & d_{22}^{E.T} & d_{23}^{E.T} & d_{24}^{E.T} & d_{25}^{E.T} & d_{26}^{E.T} & \varepsilon_{12}^T & \varepsilon_{22}^T & \varepsilon_{23}^T \\ d_{31}^{E.T} & d_{32}^{E.T} & d_{33}^{E.T} & d_{34}^{E.T} & d_{35}^{E.T} & d_{36}^{E.T} & \varepsilon_{31}^T & \varepsilon_{32}^T & \varepsilon_{33}^T \end{bmatrix} \begin{Bmatrix} T_1 \\ T_2 \\ T_3 \\ T_4 \\ T_5 \\ T_6 \\ E_1 \\ E_2 \\ E_3 \end{Bmatrix} \quad (1\text{-}9)$$

The linear theory of piezoelectricity has limitations in application that are due to different aspects as discussed here

- Electrostriction: The response of piezoelectric materials has a quadratic component which is superposed to the linear theory behavior of the material. This behavior depends on the electrostrictive coefficient which is usually lower than the linear piezoelectric coefficient but always significant as the electric field is increased.
- Depolarization: Piezoelectric materials stay polarized until they are depolarized electrically, mechanically or thermally.

  The exposure of the materials to a strong electric field of opposite polarity will depolarize the material electrically. The field strength needed to depolarize the material depends on the material grade, the length of time the material is exposed to the field and the temperature.

  When the mechanical stress on the piezoelectric material is high enough to distort the orientation and alignment of the dipole, the material becomes depolarized mechanically.

  Heating a piezoelectric material to its Curie point makes the domains disordered and the materials becomes depolarized completely.
- Frequency limitation: Natural frequency of vibration is available for all physical systems. Exposing the system to a frequency close to the natural frequency of the system will generate a oscillation very high in amplitudes. More linear compliance will be achieved at a frequency far from the natural frequency of the material.

1.4.1 Coupling factor k

As discussed fully, the piezoelectric materials couple electric and mechanical fields. Hence, it is possible to obtain electrical energy by introducing a mechanical energy as well as a

mechanical energy by introducing an electrical energy. It is then important to have a coefficient for measuring the effectiveness the electrical energy is converted into mechanical energy. This coefficient is the coupling factor k and it is defined at a frequency below the resonant frequency of the material as

$$k^2 = \frac{energy\ converted}{input\ energy\ applied\ to\ material}$$

The coupling coefficient describes energy converted in all directions. The coefficient in a specific direction is indicated by subscripts to indicate the direction in which the coefficient is calculated.

Chapter 2
Literature Review

2.1 Overview

In this chapter, a detailed literature survey on load sensors is presented. The different types of sensors and technologies employed are detailed out in this chapter. The piezoelectricity technology as applied to load magnitude determination, energy harvesting as an integral step in the applying piezoelectricity for sensing purposes is also highlighted here in this chapter. Usage of this technology for structural health monitoring is also presented. Published work of different researchers regarding energy harvesting, structural health monitoring and sensing applications are presented and discussed in this chapter. This chapter thus provides a basis for the thesis with the presentation of the work and approaches of other researchers while establishing the approach taken for this study.

2.2 Load magnitude sensing

The determination of the accurate magnitude of an applied load is often necessary in daily industrial activities. Load cells are transducers through which the value of the magnitude of the load is made known by the conversion of the potential or kinetic energy of the load to another form of energy that is then interpreted to obtain the magnitude of the load. Load cell designs are categorized based on the type of output signals they generate. The outputs are pneumatic, hydraulic or electric. They are broadly categorized as static or dynamic load sensor based on the types of loading.

The static load is the load applied to a sensor that does not vary with time [27]. There are load cells that are available in measuring this class of loading as they are described in the following subsections.

2.2.1 Strain gage sensors

The strain gage is effective in responding to high-static loads. The strain gage takes the advantage of the strain-sensitive material to return the accurate magnitude of an applied load. The strain gage uses the change in electrical resistance to measure the strain experienced by the device [21]. In shock and vibration application, the strain gage is not to determine the magnitude of the strains produced by the shock but also the entire time-history of the event. Most of the strain gage are of foil construction. The foil used is often about 0.1mm in thickness. As a result of the thinness, the foil is usually provided with a carrier medium usually paper, plastic or epoxy that performs a function of handling and simplicity of application.

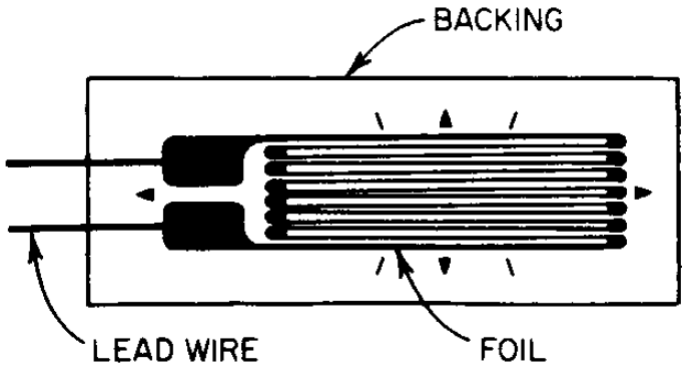

Figure 2.1:A foil strain gage. (Piersol, 2002)

The relationship between the resistance change of the gage and the strain can be expressed as

$$K = \frac{\Delta R/R}{\Delta L/L} \tag{2.1}$$

where K = gage factor of the foil, R the initial resistance, L the initial Length, ΔR and ΔL are the change in resistance and change in the length of the foil respectively.

Strain gages are established to be excellent in measuring static loads but due to their high speed of response, they are also accurate in the determination of loads under dynamic conditions.

2.2.2 Hydraulic load sensor

The hydraulic load sensor harnesses the hydraulic principle for its operation. When a load is applied on a liquid medium contained in a confined space, the pressure of the liquid increases. The increase in the pressure of the liquid is proportional to the applied force. Hence a measure of the increase in pressure of the liquid becomes a measure of the applied force when calibrated.

The main parts of a hydraulic load cell are as indicated in Figure.

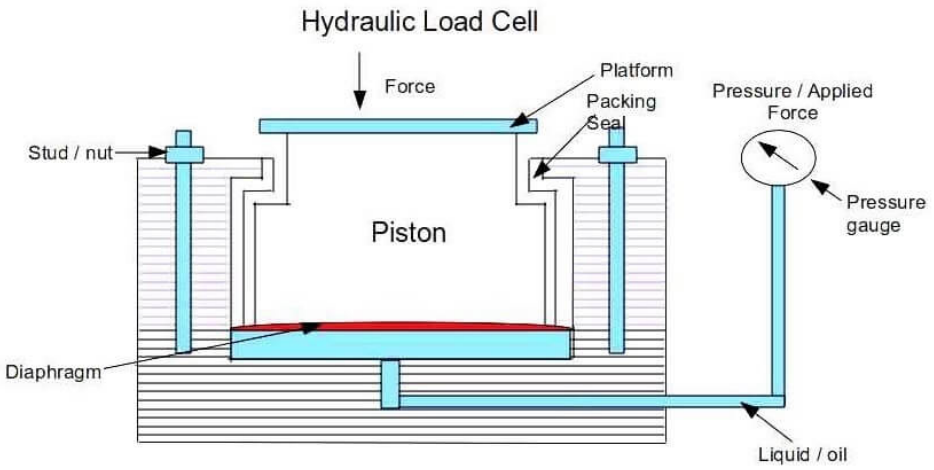

Figure 2.2: Main parts of Hydraulic load cell (Instrumentation tools)

As the hydraulic load cell is sensitive to pressure changes, the load cell needs to be adjusted to zero setting before using it to measure load [22]

The hydraulic load sensor is suited for high impact loading applications and can withstand a high overload of up to 300% in some instances without loss of accuracy.

2.2.3 Pneumatic load sensor

When a force is applied to one side of a diaphragm and an air pressure is applied to the other side of the diaphragm, some value of pressure will be necessary to exactly balance the load. This balancing pressure on the other side of the diaphragm is proportional to the applied load. The pneumatic output signal from the load cell may be read locally or transmitted by metal or plastic tubing to a remote point. The local readout of weight is usually by precision bourdon tube gage while for remote readouts, output can be transduced into electronic or digital forms.

For the accurate and successful operation, pneumatic load cells and associated weighing equipment must have a carefully regulated source of clean, dry air. A typical requirement is 10 Standard cubic feet per minute (scfm) of dry air per load cell. Pneumatic weighing system have relatively slow rates of response when the load changed incrementally.

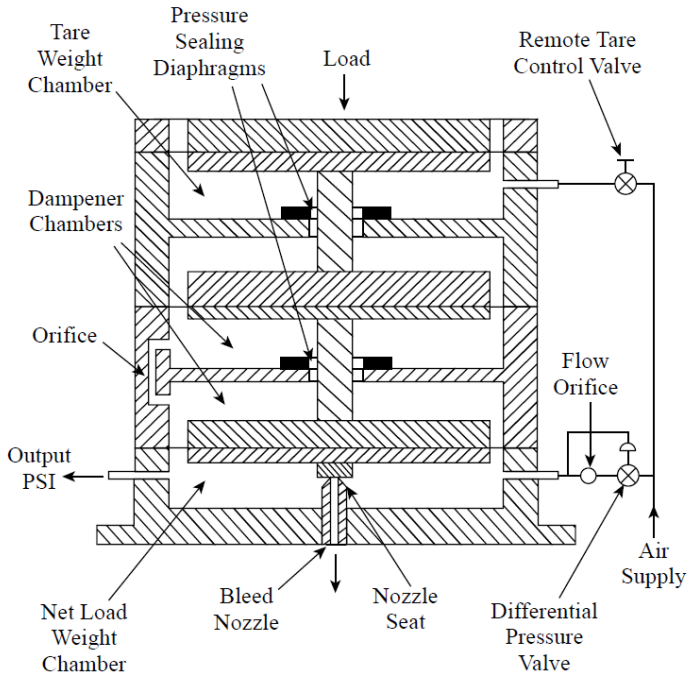

Figure 2.3: A cross section of a pneumatic load cell. (Bela, 2003)

2.2.4 Capacitance load sensor

Similar to the strain gage sensor, the basic principle involved in all capacitive load sensor is the measurement of change in capacitance resulting from the movement of an elastic element in the sensor unit. The elastic element might be a stain steel diaphragm or a metal-coated quartz element which is exposed to the load on one side and to a reference load on the other. A high-voltage, high frequency oscillator is used to energize the sensing element. Changes in applied pressure deflect the diaphragm and a bridge circuit detects the resultant change in capacitance. The two-plate design can be operated in balanced or unbalanced modes. Balanced modes incorporate a null detector while the unbalanced mode uses the ratios between the output voltage and excitation voltage to determine the loading. These are accurate to 0.1 to 0.2% of span.

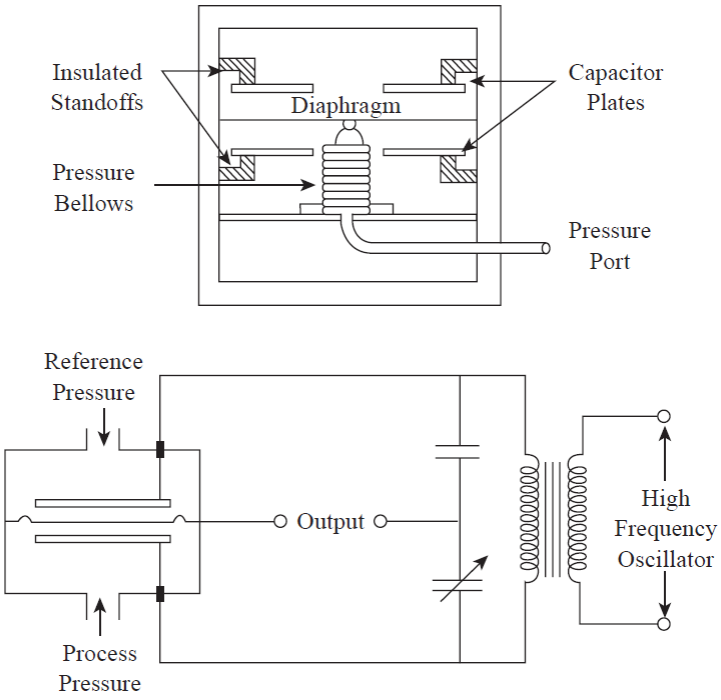

Figure 2.4: Capacitance Pressure sensor (Bela, 2003)

2.2.5 Piezoelectric Load sensor

Piezoelectric load sensor exploits the principle of piezoelectricity to return the magnitude of an applied load. These load sensors are very robust and are in wide range of industrial applications. This type of sensor is normally useful for dynamic load. When a given static force is applied, a corresponding charge across the sensor is generated but this will leak away over a given time due to imperfect insulation, internal resistance, etc. This makes the piezoelectric type of sensor not suitable for static loads. They are sensitive to dynamic changes in pressure across a wide range of frequencies and pressures [23].

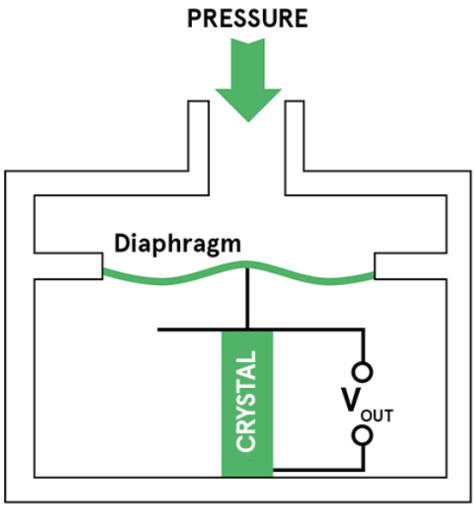

Figure 2.5: A typical piezoelectric sensor (Avnet, 2019)

Unlike the strain gage types, the piezoelectric sensor requires no external voltage or current source since they generate an output signal directly from the applied strain.

The output signal of the sensor is linear over a wide range typically 0.7kPa to 70Mpa with an accuracy of about 1% [23]. The piezoelectric sensor is rugged and robust which makes them suitable in a variety of environments. These sensors can also be used at high temperatures when piezoelectric ceramics are used in the construction of the sensors. Since the electrical signal are generated by the material itself, piezoelectric sensors are usually low powered devices.

Generally, hydraulic and pneumatic load cells are huge in size hence, the electric load cells are dominant in the sensing application. The electric load cells are used because of the easy at which energy is efficiently harvested from them.

Piezoelectric sensors have been extensively used in large variety of sensor application. Daku et al. [14] developed a theoretical model for a low-frequency, low-cost robust vibration monitoring acceleration transducer. The sensor consists of three pieces of Plexiglas, two pieces of PVDF and

a copper cylinder. The sensor was modeled as a second-order system with the copper cylinder representing the mass and the two PVDF sheets representing a spring. The completed transducer model uses a transfer function

$$H(s) = H_{mm}(s)H_{em}(s)$$

where

$$H_{mm}(s) = m\frac{\omega_n^2}{s^2 + 2\xi\omega_n s + \omega_n^2}$$

and

$$H_{em}(s) = K_f\frac{\frac{1}{K_v}s}{1+\frac{1}{K_v}s}$$

Thus giving the complete system transfer function as

$$H(s) = \left(mK_f\right)\left(\frac{\frac{1}{K_v}s}{1+\frac{1}{K_v}s}\right)\left(\frac{\omega_n^2}{s^2 + 2\xi\omega_n s + \omega_n^2}\right)$$

Strain is measured in terms of the charge generated by the element as a result of the direct piezoelectric effect. Sirohi investigated the charge generated from piezoelectric film and compared with strains from a conventional foil strain gage [15]. A pair of PZT sheets is bounded 20 mm form the root of a cantilevered aluminum beam. A dynamic beam setup was used to calibrate the piezoelectric sensors. He performed experiment by actuating the sensor from 5 – 500Hz. The strain reading from the foil gage is recorded using a conventional signal conditioning unit and the strain is calculated using standard calibration formulae.

Tolentino et al. [24] developed a piezoelectric sensor to measure the concentration of ethylene in harvested fruits to prevent rot. In the study, they fabricated a sensor by drop-casting a AgBF4/polyvinylpyrolidone composite onto a quartz crystal microbalance (QCM) which upon exposure to ethylene, the oscillation frequency decreases until a steady state is reached. This oscillation is attributed to the binding of ethylene to immobilized Ab(l) causing a change in the surface mass of the sensor. They found the sensor to be working in the linear range from 1 to 7ppm and the sensitivity limited to 51 Hz/ppm.

2.3 Energy Harvesting

At the fundamental of sensing is energy harvest since it is this harvest energy from the material of the sensor that needs to be analyzed to obtain the measured magnitude of the applied load. While energy can be harvested in various ways such as thermoelectric, photovoltaic, vibrational, etc. vibrational energy is available abundantly in the industrial environment. The Vibrational which is of interest for this study, we have the electromagnetic, electrostatic or piezoelectric energy harvesting.

2.3.1 Energy Harvesting using piezoelectricity

The sensor for measuring dynamic loading will not be possible without the ability of harvesting energy using piezoelectricity. Palosaari worked on characterizing the behavior of harvester using the mechanical strain from the heel of the foot while working [11]. Four cymbal type harvesters were investigated with the developed walking profile compression cycles and compared to sinusoidal compression cycles. The cymbal type harvester deviates from a traditional cymbal transducer having uniformly curved convex steel plate end caps. The generated voltage from actual walking was recorded, analyzed and used to create walking profile compression cycles with a computer controlled piston and at 1.19Hz compression frequency, the harvested average

power was 0.66mW which correlated with a power density of 1.37W/cm^3 for the 500 μm thick and 35mm in diameter piezoelectric element. It was found that the amount of energy harvested canstill be improved by adding more piezoelectric material to the designs, increasing the dimensions and adding layers.

Energy harvesting for the purpose of powering low power electronic sensor systems has received explosive attention in the few years. Michael and Sondipon [11] investigated the optimum design in terms of size and shape of piezoelectric patch for a cantilever beam energy harvester. The possibility of changing the shape of the transducer at the finite element nodes was considered for the optimum power from the harvester. Michael arrived at the optimum shape by iterating between several shapes taking into consideration the width and length of the sensor. It was found that for the different shape of the piezoelectric film for the transducer, the maximum power generated by each film shape is dependent on the length of the transducer giving opportunity to optimize the sensor shape to maximize the power output with a giving length of the transducer.

With the capability to print comes the flexible ability to develop complex shapes of transducers. Kamata et al. [13] worked on the development of an energy harvester made from (VDF/TrFE) copolymers using a low temperature printing technology. They were able to fabricate a piezoelectric device by a simple printing process which dramatically reduces the fabrication time and complexity as well as the avoidance of the high temperature treatment that can damage the VDT/TrFE polymer structure. Dry-cure Ag (Colloidal ink) injected by an inkjet printer was used for patterning the metal electrodes on PET films. The printed dots on the film was made 4 times to increase the density of the dots on the film after which the film was created on the printed substrate by spin coating.

2.4 Structural health monitoring

It is important to actively monitor the performance and health of structures in service and a lot of study has been done in this aspect. Monitoring the structural health of critical infrastructures and civil entities such as tall buildings, bridges, flyovers and underpass sets forth to get rid of catastrophic failure. Muhammad and Farid [16] worked on a novel multimodal bridge energy harvester using piezoelectricity. Their device consists of a permanent magnet, a wound coil, a piezoelectric plate, an airfoil and two cantilever beams attached to a base support frame. Experimentally, the sensor operated at three low frequency resonant modes, ranging from 11 to 45Hz, concentrated around 11, 38 and 43 Hz. With the design of the harvester, the loading on the bridge by the usage as well as the traffic-induced wind are being able to be measured and analyzed.

Khac-Duy et al. [17] worked on the structural health monitoring of the cable-anchorage system by using piezoelectric PZT sensors. Their method utilized the active and passive responses of piezoelectric sensors at anchorage zone and cable body, respectively. They used three steps which include the alert of any damage by monitoring the electro-mechanical impedance of anchorage zone. Both the loss of cable force and anchorage damage causes the change in structural characteristics of the anchorage zone. Then, inversely, the electro-mechanical impedance signature of anchorage zone can be utilized to detect the occurrence of those damage types. In this method, a piezoelectric (PZT) patch is usually surface-bonded to a host structure. The electrical signals of the PZT are partly controlled by mechanical effect of the host structure. By actuating the PZT with a voltage and measuring the current, the impedance can be obtained as a combined function of mechanical impedance of the host structure. The second step involves the classification of the alerted damaged by analyzing the PZT dynamic strain of the cable. The damage estimation is then made for the classified damage type.

The modelling and the experimental characterization of a hybrid harvester/actuator study was carried out by Rito et al [25]. Their work entails the development 1s a self-powered structural health monitoring system using macro-fiber composite patches. This involves the integration of the actuation, sensing and energy harvesting capabilities of the macro-fiber composite patches in the health monitoring system operating at different regimes. Their result supports the potential feasibility of the system, pointing out that the energy storage can be used for recharging a 3V-65mAh Li-on battery and also used to characterize a condition-monitoring algorithm.

The location of the patches in health monitoring is as important as the sensor itself and that is what Tarhini et al [26] worked on. They studied a novel approach for the optimization of piezoelectric wafer networks for structural health monitoring. Control points were determined such that the number of sensors for the surface area is maximized. The algorithm focused on maximizing the control points by allocating PZT wafers at optimal positions. The proposed model introduced coverage levels 2(localizing a defect) and 3(coverage of every control point) for damage detection and assessment, respectively while optimizing the locations of sensors. Using the same number of the piezoelectric wafers and higher levels, the optimization was capable of finding new PZT wafer distributions that met the coverage.

2.5 Significance of the work

The significance of this research work is to attempt to show how the principles of piezoelectricity and mechanics can be used in the health monitoring and control of infrastructures. The body of works cited above created the basis for the possibility of achieving this objective by building on the vast work of research that has been done in this field.

The following chapters present the design, simulation and notes to address these objectives.

Chapter 3
Theoretical Development

3.1 Overview

This research focuses on the development of dynamic force sensors applying piezoelectric principle. This chapter outlines and discusses in detail the development of the force sensor. In this study, the goal is to develop a force sensor that accurately and consistently measures the excitation forces in machinery or structures such as vehicle suspensions or bridge. The aim is to also to show the adaptability of the force sensor to different engineering applications right from the design phase. The presentation of the work in this chapter begins with the discussion of the concept of the sensor by summarily laying out the technique and principles followed for the sensor development for the desired force measurement. Thereafter, the concept and measurement of the volume displacement and the measurement of it is presented. The sensor development which consists of the derivation of the function representing the shape of the PVDF film is presented. Finally, the procedure for the determination of the excitation force on the sensor which is found from the electrical charge obtained from the shaped film is presented and discussed concluding the theoretical development of the sensor.

3.2 Sensor concept and configuration

A sensor is a device that receives a stimulus and responds with an electrical signal as discussed in Fraden [32]. In this work, the stimulus of interest is the force which magnitude is to be determined. The broad depiction of the sensor is shown in Fig. 3.1.

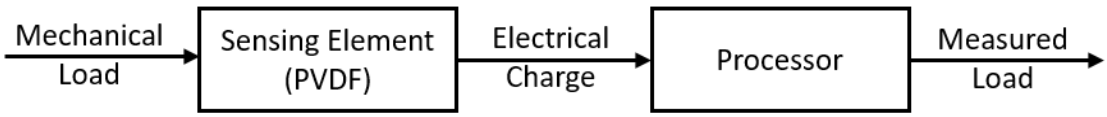

Figure 3.1: Schematic representation of the sensor system

The PVDF sensor system is expose to the load stimulus, the resulting electrical charge is analyzed to obtain the magnitude of the applied load. The sensor consists of two major parts. The primary part of the sensor system is the piezoelectric sensing element and the second part is the substrate upon which the piezoelectric sensing element is attached. The thickness of the film is very small compared to the thickness of the substrate such that it can be assumed that the mechanical distortion of the substrate is not affected by the attachment of the piezoelectric film.

The volume displacement approach is employed in the development of the sensor. Using this approach, the sensor system is developed such that the charge from the PVDF film is equal to the volume displacement of the substrate. Hence, if we know the charge from the film, then we can obtain the profile of the excitation force.

Let $\boldsymbol{P}e^{i\omega t}$ be the dynamic force we are interested in obtaining and assumed to be applied as indicated in Fig. 3.2. The force produces deflection in the beam substrate which generates a mechanical strain that is subsequently applied to the PVDF film. Applying the principle of piezoelectricity, the resulting strain causes the PVDF film to generate an electrical charge. In this application, it is desired that the generated charge be proportional to the volume displacement of the beam.

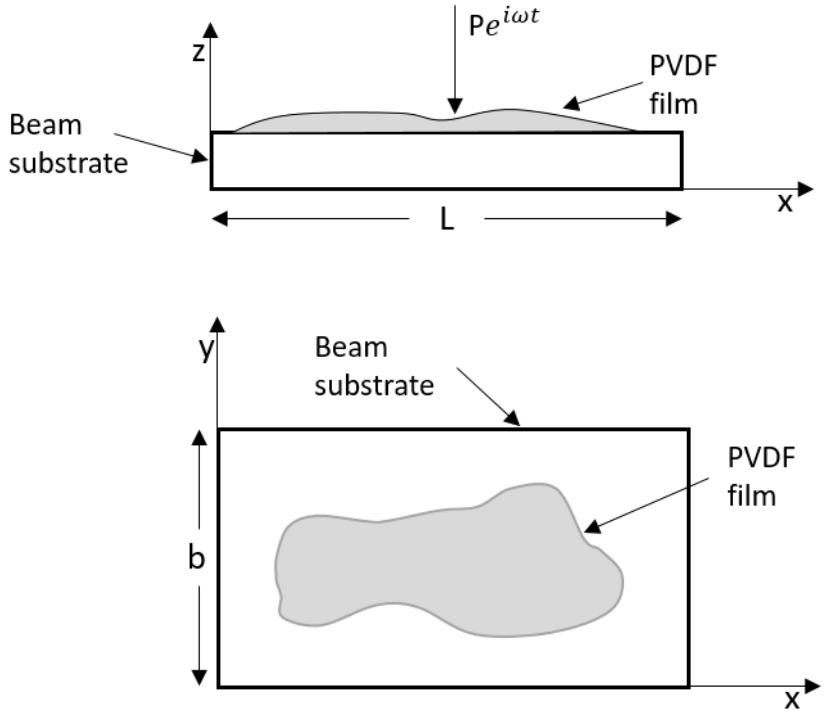

Figure 3.2: Configuration of the sensor

If the measured charge from the PVDF film is represented by q and the volume displacement of the beam by D, then applying the concept of the sensor described, we can write

$$q = D \tag{3-1}$$

3.3 Volume displacement

The volume displacement of a beam is the swept region of the beam from the unexcited position to the deflected position of the beam due to the action of an external stimulus. As depicted in Fig. 3.3, if the deflection of the beam under any external stimulus is represented by $w(x)$, then the volume displacement D will be the deflection area (the hatched portion of the diagram)

multiplied by the width b of the beam. This deflection area can be found by carrying out the integration of $w(x)$ over the length L of the beam.

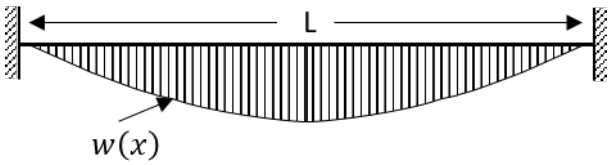

Figure 3.3: Deflection of the sensor

$$D = b\int_0^L w(x)dx \tag{3-2}$$

3.4 Volume Displacement Measurement

Researchers have worked on the measurement of the volume displacement of sound sources in an attempt to cancel or minimize the sound power generated from those sources. Johnson and Elliot [29] worked on the cancellation of the volume velocity as an active control strategy for reducing the transmission of sound through a flexible panel by using a piezoelectric actuator placed on the flexible panel to measure and serve as a secondary driving source to force the panel in the counter direction to reduce the deflection. The volume displacement measurement is important in our sensor development since we need to couple the mechanical strain with the electrical response of the piezoelectric material for the accurate functioning of the sensor. Their

technique of utilizing charges from piezoelectric materials attached to a vibrating panel is adopted in this research for our sensor.

The primary concept adopted in this work is the application of the volume displacement technique to determine the profile of an external stimulus acting on the sensor.

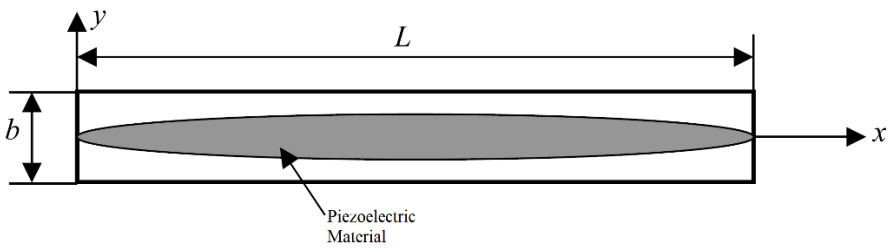

Figure 3.4: Beam with a shaped piezoelectric material

Considering the sensor configuration with a beam of length L, width b and thickness h on which a piezoelectric film is attached as shown in Fig. 3.4.

Lee and Moon [31] found that the charge generated from a single span of piezoelectric material attached to a beam of length L such that the deflection of the beam is assumed the same as the deflection of the piezoelectric material is

$$q = \frac{(h + h_s)e_{31}}{2} \int_0^L F(x) \frac{\partial^2 w}{\partial x^2} dx \qquad (3 - 3)$$

where

q is the charge generated from the piezoelectric film

e_{31} is film stress/charge coefficient

w(x) is the deflection of the beam

F(x) is the shape function of the piezoelectric film

h is the thickness of the beam

h_s is piezoelectric material thickness

Eqn. (3 - 3) can be integrated by parts as

$$q = -ze_{31}\left\{\left[F(L)\frac{\partial w(L)}{\partial x} - \frac{\partial F(L)}{\partial x}w(L)\right] - \left[F(0)\frac{\partial w(0)}{\partial x} - \frac{\partial F(0)}{\partial x}w(0)\right] + \int_0^L \frac{\partial^2 F(x)}{\partial x^2}w(x)dx\right\} \quad (3 - 4)$$

where z = -$(h + h_s)/2$

To completely evaluate this equation, we considered the clamped-clamped boundary conditions for a beam which are

$$w(0) = 0 \quad (3 – 5a)$$

$$w(L) = 0 \quad (3 – 5b)$$

$$\frac{\partial w(0)}{\partial x} = 0 \quad (3 – 5c)$$

$$\frac{\partial w(L)}{\partial x} = 0 \quad (3 – 5d)$$

Applying these conditions to Eqn. (3 - 4), we obtain

$$q = -ze_{31}\int_0^L \frac{\partial^2 F(x)}{\partial x^2} w(x)dx \qquad (3 - 6)$$

Assuming a quadratic shape function $F(x)$ for the film as in Eqn. (3 - 7) shows

$$F(x) = Ax^2 + Bx + C \qquad (3 - 7)$$

If the film extends to both clamped boundary, then

at $x = 0, F(0) = 0$ which yields $C = 0$ and

at $x = L, F(L) = 0$ which yields $B = -AL$.

Substituting the values of the coefficients back into Eqn. (3 - 7), yields

$$F(x) = A(x^2 - Lx) \qquad (3 - 8)$$

Substituting Eqn. (3 - 8) into Eqn. (3 -6), we obtain

$$q = -2Aze_{31}\int_0^L w(x)dx \qquad (3 - 9)$$

Using Eqn. (3 - 2) and (3 - 9) into Eqn. (3 - 1), we obtain

$$A = \frac{b}{2Aze_{31}} \qquad (3 – 10a)$$

$$A = \frac{b}{(h + h_s)e_{31}} \qquad (3 - 10b)$$

Eqn.. (3 -10b) is the expression for the coefficient A of the shape function $F(x)$.

The shape function $F(x)$ is the line bounding the film on the x-y plane of the beam. Thus, $F(x)$ Is developed such that a half of the plane is bounded while the other half is bounded by - $F(x)$.

Fig. 3.5 represents the fully designed sensor.

Figure 3.5: Shaped piezoelectric film for the fixed-fixed boundary condition

3.5 Sensor Equations

This section discusses the derivation of the sensor equation under various force profiles. The equations of the sensor are important to be known as they describe the principle upon which the functionality and the effectiveness of the sensor is based. With a known generated charge q from the film due to the action of an excitation and the expression of the volume displacement D of the substrate the excitation force can be determined. The volume displacement of a beam under a static force will first be developed and discussed. Just then the volume displacement under harmonic excitation will be developed. Finally, the volume displacement under a random excitation spanning a range of frequencies will also be presented and discussed in this section.

3.5.1 Static Excitation

The assumption made for the analysis presented in this section is that the force acting on the beam is a point load and acting at the middle as shown. A fixed beam at both ends subjected to a static force P acting at the center undergoes a deflection represented by

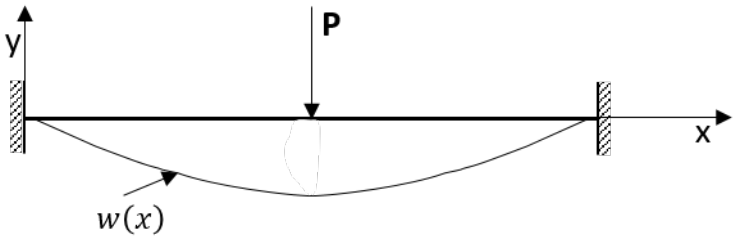

Figure 3.6: Beam deflection under static load

$$w(x) = -\frac{Px^2}{48EI}(3L - 4x)\,, (0 \leq x \leq \frac{L}{2}) \qquad (3 - 11)$$

where

E is the modulus of elasticity of the beam material

I is the moment of inertia of the beam

Substituting the deflection equation of equation (3 - 11) into equation (3 - 2), we obtain

$$D = 2b\int_0^{\frac{L}{2}}\left[\frac{Px^2}{48EI}(3L - 4x)\right]dx \qquad (3 - 12)$$

Evaluating the integral in Eqn. (3 – 12), we obtain

$$D = \frac{PbL^4}{384EI} \tag{3 - 13}$$

Using the relationship in Eqn. (3 - 1), we equate Eqn. (3 - 13) representing the volume displacement to the charge from the film. Hence, we obtain

$$q = \frac{PbL^4}{384EI} \tag{3 - 14}$$

Thus

$$P = \frac{384EIq}{bL^4} \tag{3 - 15}$$

Eqn. (3 - 15) is the expression for the response of the sensor as a result of an unknown static force acting on it. Due to the time constant, the charge leakage from the imperfect insulation and internal resistance of the sensor, the charge from a static force cannot be measured adequately to obtain the magnitude of the force. Hence, piezoelectric materials are not usually suitable for static force applications.

3.5.2 Harmonic Excitation

If the load in Fig. 3.6 is a dynamic force of the form $\boldsymbol{P}e^{i\omega t}$, the deflection of the beam (Rao 2011) is

$$w(x,t) = \frac{P}{\rho A}\sum_{n=1}^{\infty}\frac{\{\sinh(\beta_n a) - \sin(\beta_n a) + \alpha_n[\cosh(\beta_n a) - \cos(\beta_n a)]\}\sin(\omega t)}{[B(\omega_n^2 - \omega^2)][W_n(x)]^{-1}} \qquad (3 - 16)$$

where ω is the frequency of excitation of force

a is $\frac{L}{2}$

ω_n is the natural frequencies of the beam

A is the cross-section area of the beam

ρ is the density of the material of the beam material

E is the modulus of elasticity of the beam material

I is the moment of inertia

α_n is $\frac{\sinh\beta_n l - \sin\beta_n l}{\cos\beta_n l - \cosh\beta_n l}$

$W_n(x) = \sinh\beta_n x - \sin\beta_n x + \alpha_n(\cosh\beta_n x - \cos\beta_n x)$ and

β_n is $\left(\frac{\rho A\omega_n^2}{EI}\right)^{1/4}$

B is $\int_0^l W_n^2(x)dx$

Eqn. (3 - 16) is obtained using the mode superposition principle and the frequency of the force is limited to the first natural frequency of the beam substrate.

We obtain the expression of the volume displacement of the beam for the dynamic force by integrating Eqn. (3 - 2) while substituting for $w(x)$ from Eqn. (3 - 16) to obtain

$$D = \frac{bP}{\rho A}\sum_{n=1}^{\infty}\int_{0}^{L}\frac{\{\sinh(\beta_n a) - \sin(\beta_n a) + \alpha_n[\cosh(\beta_n a) - \cos(\beta_n a)]\}\sin(\omega t)}{[B(\omega_n^2 - \omega^2)][W_n(x)]^{-1}}dx \qquad (3 - 17a)$$

$$D = \frac{bP}{\rho A}\sum_{n=1}^{\infty}\frac{\{\sinh(\beta_n a) - \sin(\beta_n a) + \alpha_n[\cosh(\beta_n a) - \cos(\beta_n a)]\}\sin(\omega t)}{[(\omega_n^2 - \omega^2)B\beta_n][\alpha_n \sinh(\beta_n L) - \alpha_n \sin(\beta_n L) + \cosh(\beta_n L) + \cos(\beta_n L) - 2]^{-1}} \qquad (3 - 17b)$$

Using Eqn. (3 - 1), the expression for the volume displacement D in Eqn. (3 - 17b) is the expression of the charge q in response to the excitation $\boldsymbol{P}e^{i\omega t}$ acting on the sensor.

The expression for the unknown force $\boldsymbol{P}$ is then derived by following the same approach employed for the static force.

From Eqn. (3 – 17b), we can write

$$f(\omega) = \sum_{n=1}^{\infty}\frac{\{\sinh(\beta_n a) - \sin(\beta_n a) + \alpha_n[\cosh(\beta_n a) - \cos(\beta_n a)]\}^{-1}}{[\alpha_n \sinh(\beta_n L) - \alpha_n \sin(\beta_n L) + \cosh(\beta_n L) + \cos(\beta_n L) - 2][(\omega_n^2 - \omega^2)B\beta_n]^{-1}} \qquad (3 - 18)$$

and

$$K = \frac{\rho A}{b} \tag{3 - 19}$$

We obtain the expression for the measured force as

$$P = qKf(\omega)^{-1} \tag{3 - 20}$$

Eqn. (3 - 20) represents the unknown excitation the profile of which is to be determined from the sensor given the charge q from the film.

3.7 Sensor Development Assumptions and Limitations

Piezoelectric materials especially ceramics with thicker dimensions are anisotropic in nature. They possess properties that are of different values at different direction. Since this study was performed with a piezoelectric film having a thin thickness, it is assumed that the properties of the film used one dimensional and that they are the same across all spatial direction and the beam theory can be applied.

It is also assumed that the developed strain in the substrate is transferred directly unto the film without absorption or altering by the adhesion material between the film and the substrate. This assumption is necessary as to ensure the accuracy of the sensor in measuring the applied force.

While it is possible to develop a piezoelectric sensor to be used for a static load, the development of the proposed sensor is limited to the measurement of dynamic force with the excitation frequency lesser than the first natural frequency of the beam substrate.

Chapter 4
Numerical Validation

4.1 Overview

In this chapter, the numerical validation of the sensor designed in chapter three is presented. A detailed description of the materials employed as well as their properties, the reasons behind those choices and the simulation tools used in validating the output numerically are discussed in this chapter. This stage of the study is necessary because we need to use simulation tools available to confirm that the methods used as well as the assumptions made when developing the sensor are acceptable before we proceed to construct the sensor for experimental validation. Finally, the results from the simulation tools are compared to the expected results.

4.2 Material Selection

At the heart of this research are the materials employed in designing and constructing the sensor system. In this section, the material details of the sensing element and the beam substrate upon which the sensing element is attached to complete the sensor is discussed. The first part of this section describes the material of the sensing element of the sensor system which is a piezoelectric film and the second part discusses the beam substrate upon which the sensing piezoelectric element is attached.

4.2.1 Piezoelectric Material Selection

The piezoelectric material chosen for this research is the PolyVinyliDene Fluoride (PVDF). PVDF is chosen as our choice of material because it is highly flexible and easily shaped to obtain the desired form for the purpose of this research. There are two metallization common options commercially: the silver ink and the sputtered metallization [16]. The sputtered metallization is generally thinner, brittle and applicable where low mass is critical. The silver ink option offers

great flexibility and is ideal for applications where mechanical stress is used. The silver ink metallization option of the PVDF is used for this research.

The properties of the PVDF are shown in Table 4.1.

Table 4.1: Properties of PVDF film

Symbol	Parameter	PVDF	Units
t	Thickness	9, 28, 52, 110	µm
d_{31}	Piezo Strain Constant	23	10^{-12} $\frac{m/m}{V/m}$ or $\frac{C/m^2}{N/m^2}$
d_{33}		-33	
g_{31}	Piezo Stress constant	216	10^{-3} $\frac{V/m}{N/m^2}$ or $\frac{m/m}{C/m^2}$
g_{33}		-330	
k_{31}	Electromechanical Coupling Factor	12%	
k_t		14%	
C	Capacitance	380 for 28 µm	pF/cm^2 @ 1KHz
E	Young's Modulus	2 -4	10^9 N/m^2
V_o	Speed of Sound: Stretch	1.5	10^3 m/s
	Thickness	2.2	
P	Pyroelectric Coefficient	30	10^{-6} C/m^2 ^{O}K
ε	Permittivity	106 – 113	10^{-12} F/m
ε/ ε_o	Relative Permittivity	12 – 13	
ρ_m	Mass Density	1.78	10^3 kg/m
ρ_e	Volume Resistivity	$>10^{13}$	Ohm Meters

R	Surface Metallization Resistivity	0.1	Ohms/square for Ag Ink
tan δ_e	Loss Tangent	0.02	@ 1KHz
Y	Yield Strength	45 – 55	10^6 N/m^2
T	Temperature Range	-40 to 100	^{O}C
A_m	Water Absorption	<0.02	% H_2O
V_{max}	Maximum Operating Voltage	750	V/mil (V/µm)
V_b	Breakdown Voltage	2000	V/mil (V/µm)

4.2.2 Beam Substrate Selection

The beam substrate material selected for the sensor is Aluminum. The substrate is needed to serve as a support for the film and for the strain developed to be transmitted to the PDVF film. The substrate is of the fixed-fixed boundary condition and this is the boundary condition on which the theoretical development is based. The dimensions and properties of the beam substrate are as presented in Table 4.2

Table 4.2: Dimensions of beam substrate

Parameter	**Symbol**	**Value**	**Unit**
Length	L	230	mm
Width	b	30	mm
Thickness	h	2	mm
Density	ρ	2700	kg/m^3
Yield Strength	Y	145	MPa
Modulus of Elasticity	*E*	68.9	GPa

4.3 Finite Element Analysis and Simulation

The advancement of science and technology has led to the need to finding solutions for different types of problems. This makes it necessary for a thorough engineering analysis to be done before these engineering solutions are made available for use. A powerful tool for these analysis is using numerical methods in which finite element method has gained its reputation and has become an essential step in the design process. This step of the research involves the use of the finite element technique to obtain the behavior of the sensor as close to the service condition as possible. The finite element analysis and simulation performed in this section was done using ANSYS. This step of the research is done to validate the derived functionality of the sensor to provide the ground work for the experimental work to be done afterwards. This simulation is done by a combination of analysis types. The steps followed in performing this analysis in ANSYS include defining the engineering material properties for each of the element of the sensor to be used in the simulation, the geometry representing each of the sensor objects are generated and the engineering material properties defined assigned to them. The modal analysis was done to obtain the natural frequency of the sensor then the transient structural analysis performed on the sensor to obtain the voltage for the determination of the measured applied force.

4.3.1 Geometry generation

The geometry for the analysis was generated from the ANSYS mechanical modeler. The substrate of the sensor was designed to ensure we can fasten the sensor firmly for the experimental runs of the study. The film element was then modeled on the substrate by joining series of consecutive points that follow the shape function of the film. The points generated for the sensor film is as shown in Fig. 4.1 and the completed sensor model is shown in Fig. 4.2

Figure 4.1: Points representing the sensor film in ANSYS

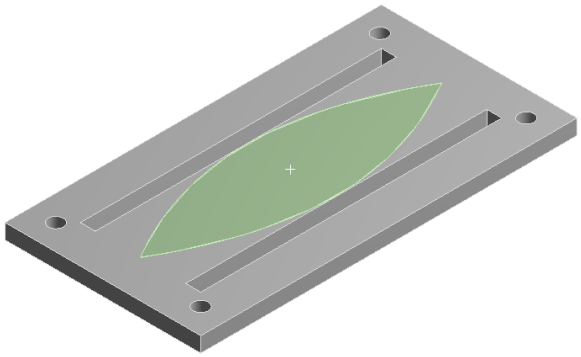

Figure 4.2: Measured random force and the excitation force

4.3.2 Meshing

The meshing of the sensor was performed automatically using the ANSYS workbench application. The substrate of the sensor was meshed using element size sufficient for the solution to converge ensuring the voltage obtained from the film is a representation of the voltage by the volume displacement of the beam substrate.

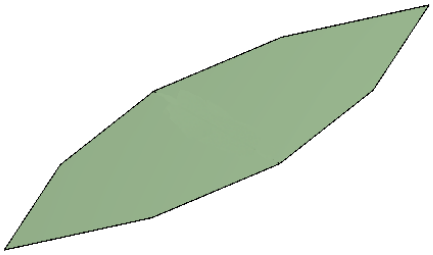

Figure 4.3: Film meshing

Figure 4.4: Sensor substrate meshing

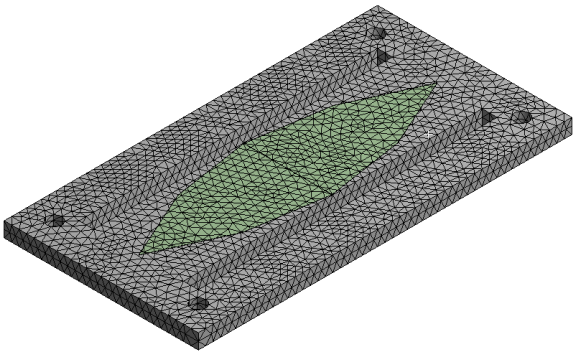

Figure 4.5: Completed meshed sensor

4.3.3 Boundary Condition and Loading

Solving the simulation problem of the sensor requires applying an appropriate boundary condition that represents the real-life activity of the sensor. A fixed support is applied to the fastening hole of the sensor presenting a clamped-clamped beam condition. The force P used in this simulation is a point load acting at the center of the sensor as shown in Fig. 4.6

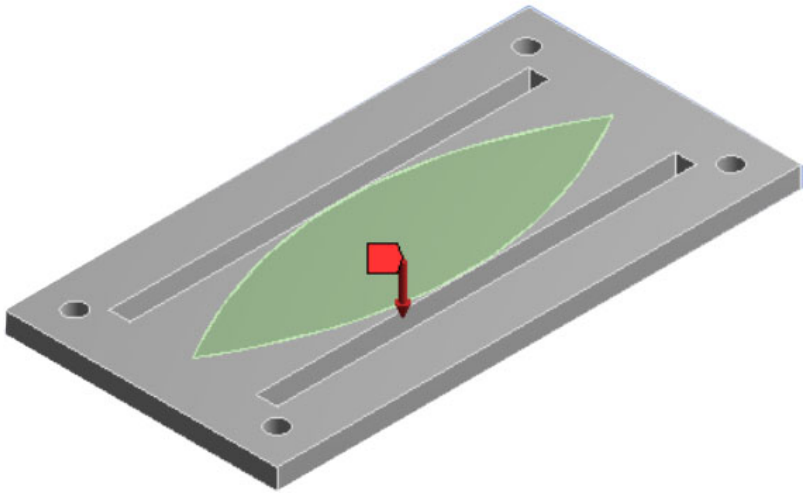

Figure 4.6: Boundary condition and sensor loading

Details of "Force"	
Scope	
Scoping Method	Geometry Selection
Geometry	1 Vertex
Definition	
Type	Force
Define By	Components
Coordinate System	Global Coordinate System
X Component	0. N (step applied)
Y Component	= 2*sin(208800*time)
Z Component	0. N (step applied)
Suppressed	No
Function	
Unit System	Metric (m, kg, N, s, V, A) Degrees rad/s Celsius
Angular Measure	Degrees
Graph Controls	
Number Of Segments	500.

Figure 4.7: Simulation force details

Details of "Piezoelectric Body"	
Geometry	
Scoping Method	Geometry Selection
Geometry	1 Body
Definition	
Material Definition	Simplified
Polarization Axis	Y
Permittivity Constant	8.854E-12 [A A sec sec sec sec kg^-1 m^-1 m^-1 m^...
PIEZ e31	0.00011286 [A sec m^-1 m^-1]
PIEZ e33	-0.00028421 [A sec m^-1 m^-1]
PIEZ e15	-0.0001222 [A sec m^-1 m^-1]
DPER ep11	8
DPER ep33	12
RSVX	0 [kg m m m A^-1 A^-1 sec^-1 sec^-1 sec^-1]
RSVY	0 [kg m m m A^-1 A^-1 sec^-1 sec^-1 sec^-1]
RSVZ	0 [kg m m m A^-1 A^-1 sec^-1 sec^-1 sec^-1]

Figure 4.8: Simulation piezoelectric body details

4.3.4 Results

The entire finite element analysis of the sensor was carried out in ANSYS workbench. A fixed support boundary condition was applied to the fastening hole on the substrate of the sensor to effect the fixed boundary condition of the sensor. The properties of the piezoelectric film used in the simulation of the sensor is provided in the appendix. Modal analysis of the sensor was performed to obtain the first natural frequency of the sensor. This was fed in to the transient analysis of the sensor to obtain the voltage generated while limiting the usage of the sensor to the first natural frequency of the sensor. The steady state simulation of the transient analysis of the sensor was obtained.

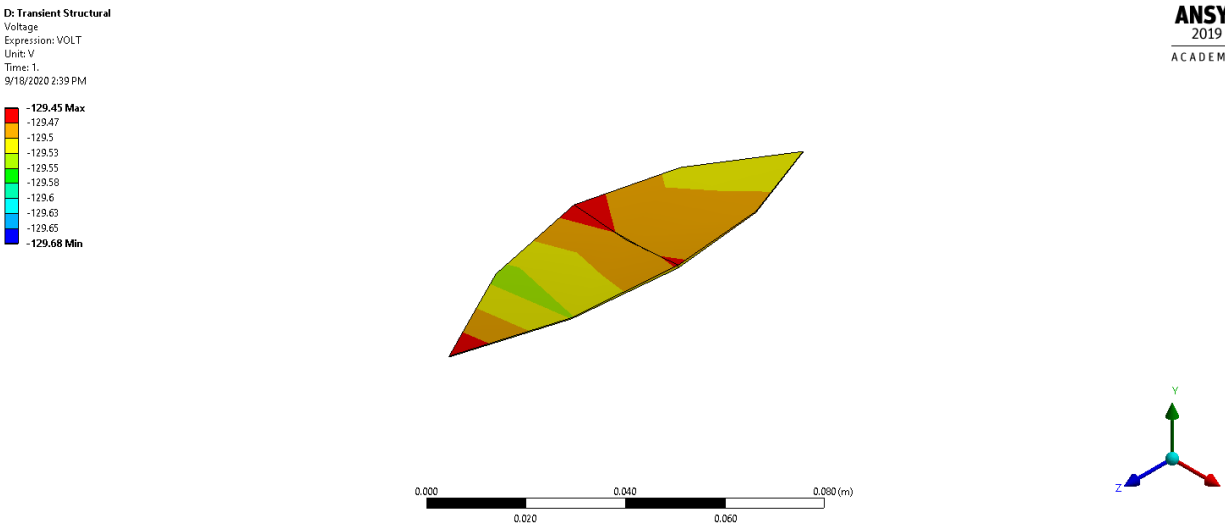

Figure 4.9: simulated output voltage from the sensor

The sensor equation from the simulation is

$$\boldsymbol{P_m} = qf(\omega)^{-1} \tag{4 – 1}$$

where

$$f(\omega) = \frac{1}{-0.00051\omega + 0.18}$$

The comparison of the measured force and the excitation force on the sensor is shown in Fig. 4.10

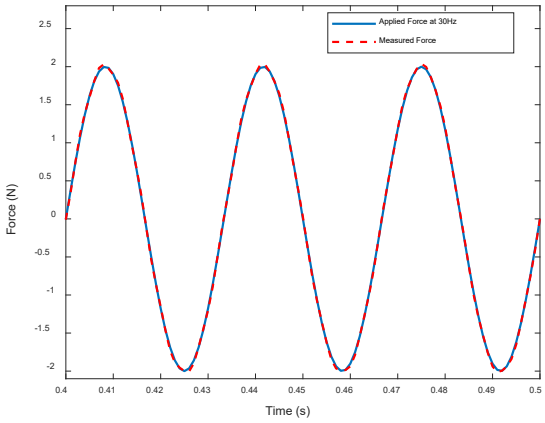

Figure 4.10a: Result at 30Hz

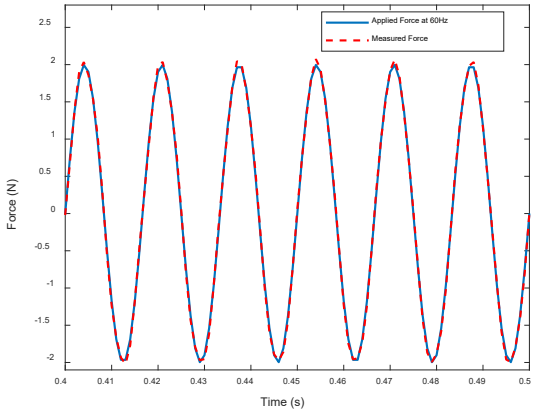

Figure 4.10b: Result at 60Hz

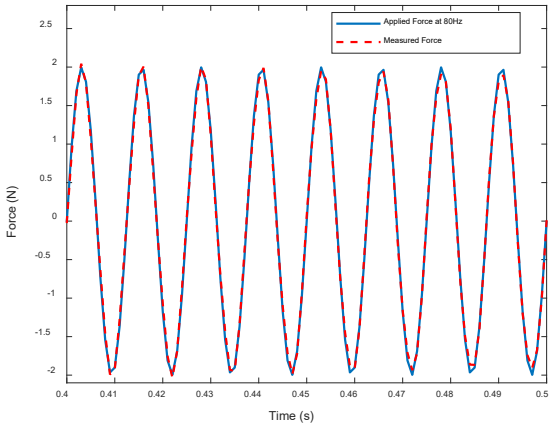

Figure 4.10c: Result at 80Hz

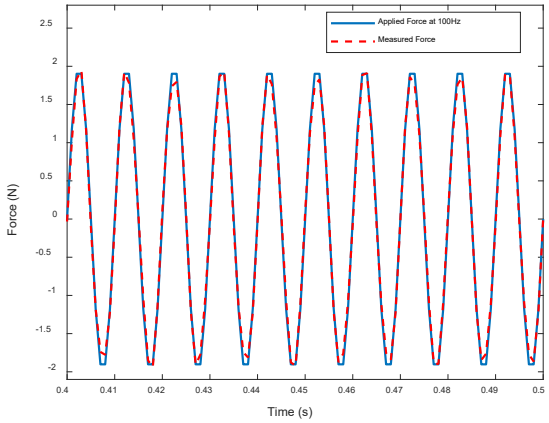

Figure 4.10d: Result at 100Hz

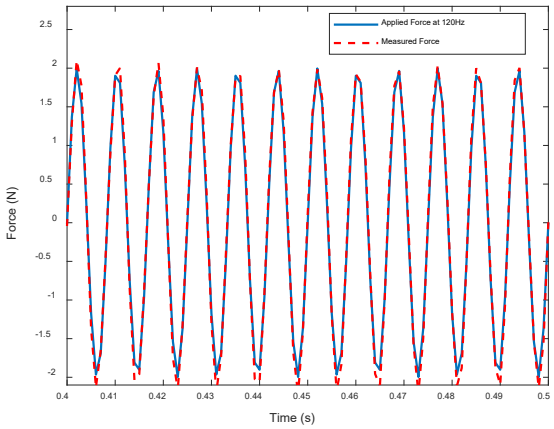

Figure 4.10e: Result at 120Hz

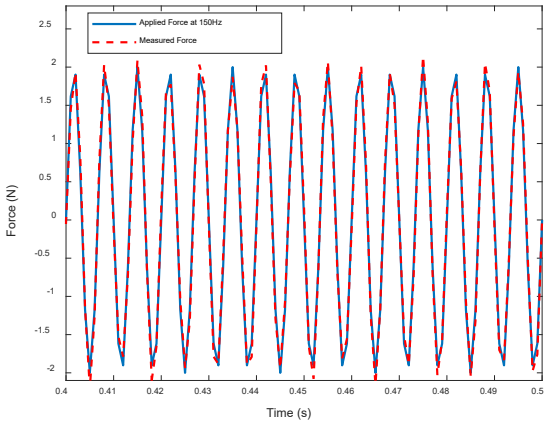

Figure 4.10f: Result at 150Hz

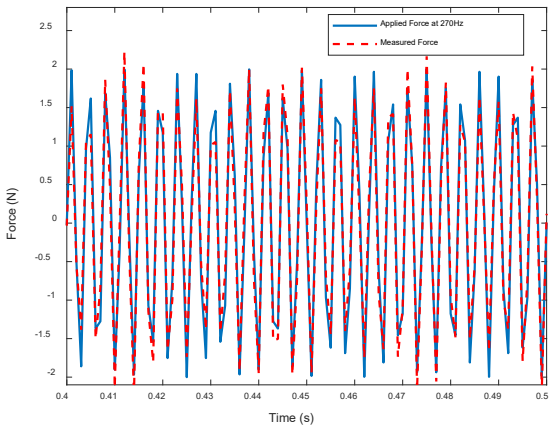

Figure 4.10g: Result at 270Hz

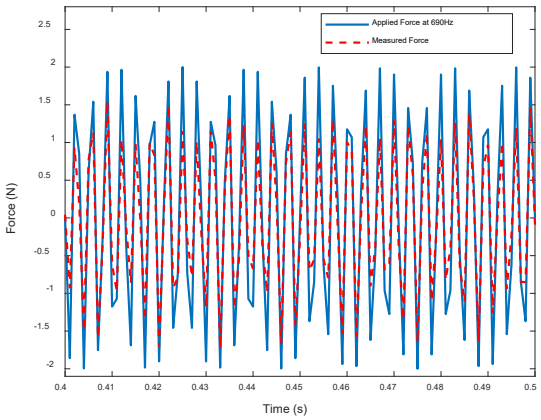

Figure 4.10h: Result at 690Hz

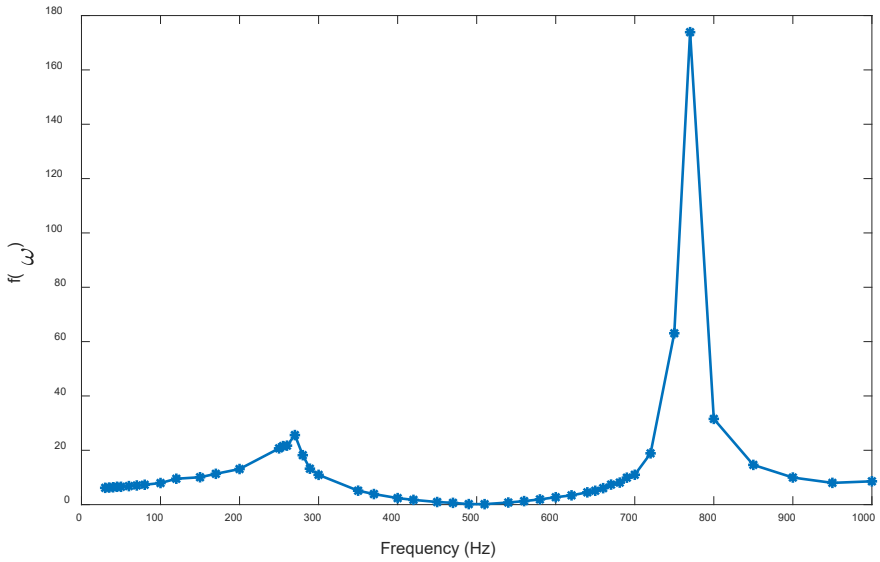

Figure 4.10i: Sensor frequency response

The simulation of the response of the sensor to a random excitation is shown in Fig. 4.22

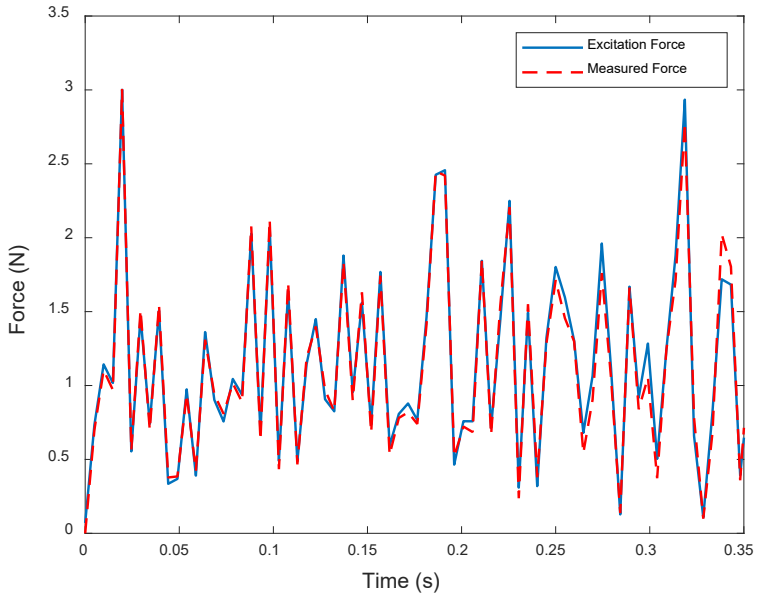

Figure 4.11: Sensor response to random excitation

4.3.5 Measurement Error

The deviation of the measure force from the sensor from the actual value of the force is important to be known for an informed decision making effort. The error of the sensor for each of the frequencies if shown in the generated figures of Fig. 4.21.

The error measure error of the sensor is determining using Eqn. (4-1)

$$\%\ Error = \frac{Maximum\ Force - Measured\ Force}{Maximum\ Force} \times 100 \qquad (4-2)$$

Chapter 5
Experimental Validation

5.1 Overview

The development and the theoretical validation of the sensor has been discussed in preceding chapters 3 and 4 of this thesis. In this chapter, the fabrication of the sensor, experimental setup and the experimental run are presented. In this phase of the research, the equations developed and the simulation result of the sensor is attempted to be confirmed using the material employed in the theoretical development and the simulation. The components of the sensor which are the aluminum substrate and the PVDF film are first prepared, assembled and mounted on a stand. The experiment equipment is assembled for the experimental run as outlined and discussed in this chapter.

5.2 Sensor Fabrication

The sensor consists of two main components; the Aluminum beam substrate which serves to support the sensing element and the PVDF film which is the main sensing element of the sensor. The design from which the aluminum substrate was machined was made using SolidWorks as shown in Fig. 5.1.

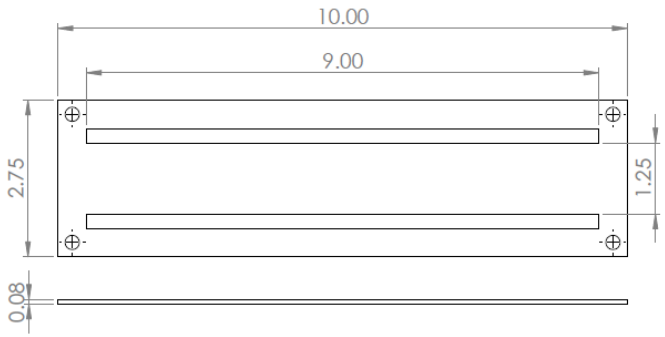

Figure 5.1: Sensor substrate design

As shown in Fig. 5.1, the design of the sensor substrate is provided with four fastening holes to ensure the sensor is fastened properly to the foundation to achieve the fixed boundary condition on which the sensor was developed as close as possible. The design was used to machine out the substrate as shown in Fig. 5.2.

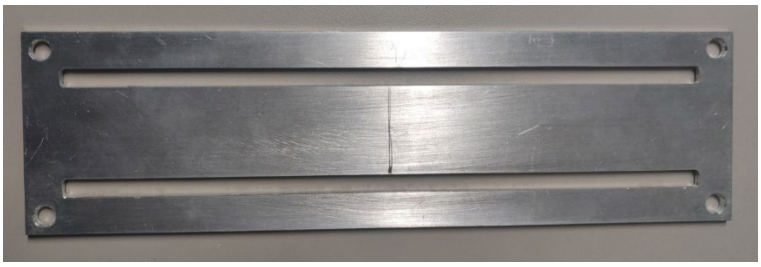

Figure 5.2: Machined Sensor substrate

The second component of the sensor which is the PVDF sensing element was cut out from a film following the shape function developed in chapter to obtain the sensing film attached to the machined sensor substrate to obtain the completed sensor as shown in Fig. 5.2.

Figure 5.3: Completed Sensor

The completed sensor is as shown in Fig. 5.3. The PVDF film is designed and cut so that the volume displacement of the substrate is proportional to the voltage from the film and thus the excitation force can be obtained using the developed sensor equations.

5.3 Experimental Setup

The successful running of the experiment to determine the accurate functioning of the sensor is dependent on a number of equipment and their connections. This section is devoted to the presentation of the setup of these equipment and their connections. The equipment used are

a) Dynamic Signal Analyzer: The analyzer is manufactured by the Agilent Technologies and it is a crucial equipment in the experimental setup. The analyzer makes it possible to select the type as well as the magnitude of the excitation force. It also stores the experiment data for post processing.

Figure 5.4: Dynamic Signal Analyzer

b) Amplifier: The amplifier interprets the signal from the analyzer and actuates the shaker in response to the signal

Figure 5.5: Signal Amplifier

c) Shaker: The Shaker is used to achieve the excitation of the sensor based on the input signal from the signal analyzer.

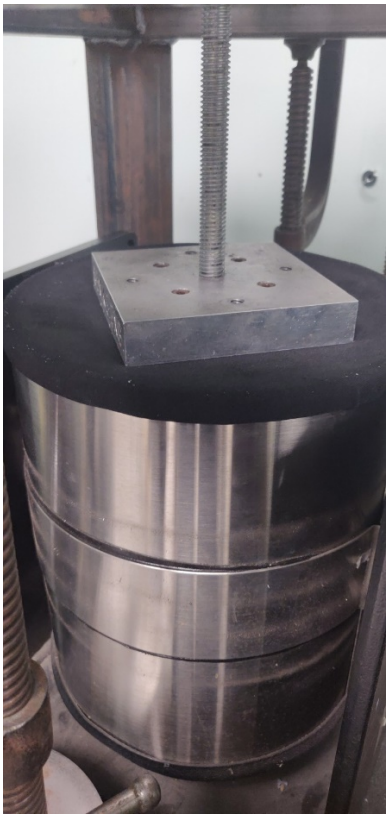

Figure 5.6: Shaker Unit

d) Recording Unit: The recording unit manufactured by TEAC is an equipment used primarily for the collecting of the experiment data. This unit is integrated with the PC for direct recording of the useful data on the disk drive.

Figure 5.7: Data Recording Unit

e) Accelerometer and Force sensor: The accelerometer and the force sensor are manufactured by PCB and are sensors for product testing. The accelerometer is used to measure the acceleration of a point on our sensor from which the displacement of the point is obtained while the force sensor was used to measure the input force from the shaker on the designed sensor.

The schematic of the experimental setup is shown in Fig. 5.8

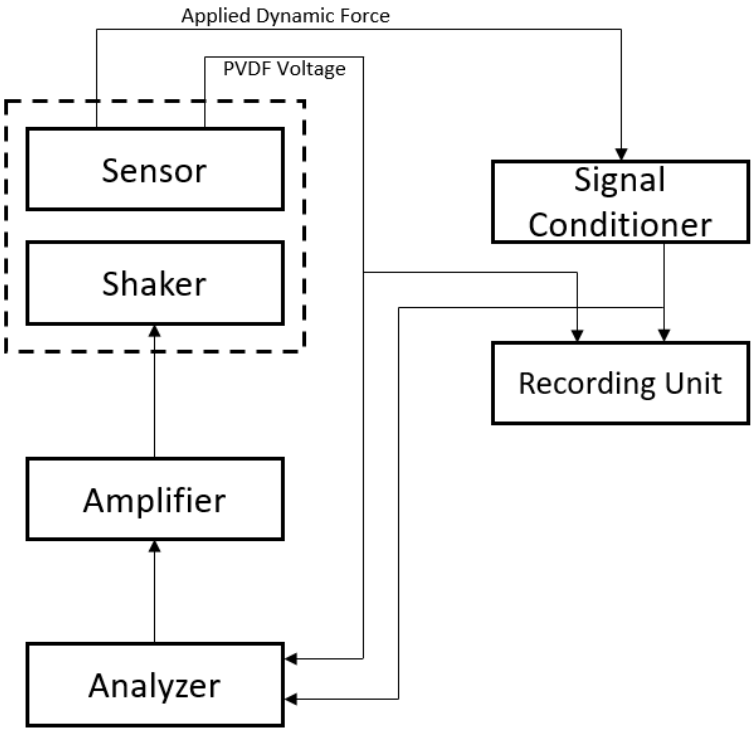

Figure 5.8: Setup Schematic

The arrangement and the setup of the equipment is as shown in the schematic in Fig. 5.8. The Signal analyzer which is the source of the experiment excitation force is connected to the amplifier which interpret and sends the chosen signal to the shaker. The shaker excites the designed sensor via a force sensor which collects the profile of the excitation force. The voltage from the PVDF sensor is then routed to the recording unit as well as the signal analyzer for data recording and post processing. The actual setup of the equipment for the experiment is shown in Fig. 5.9.

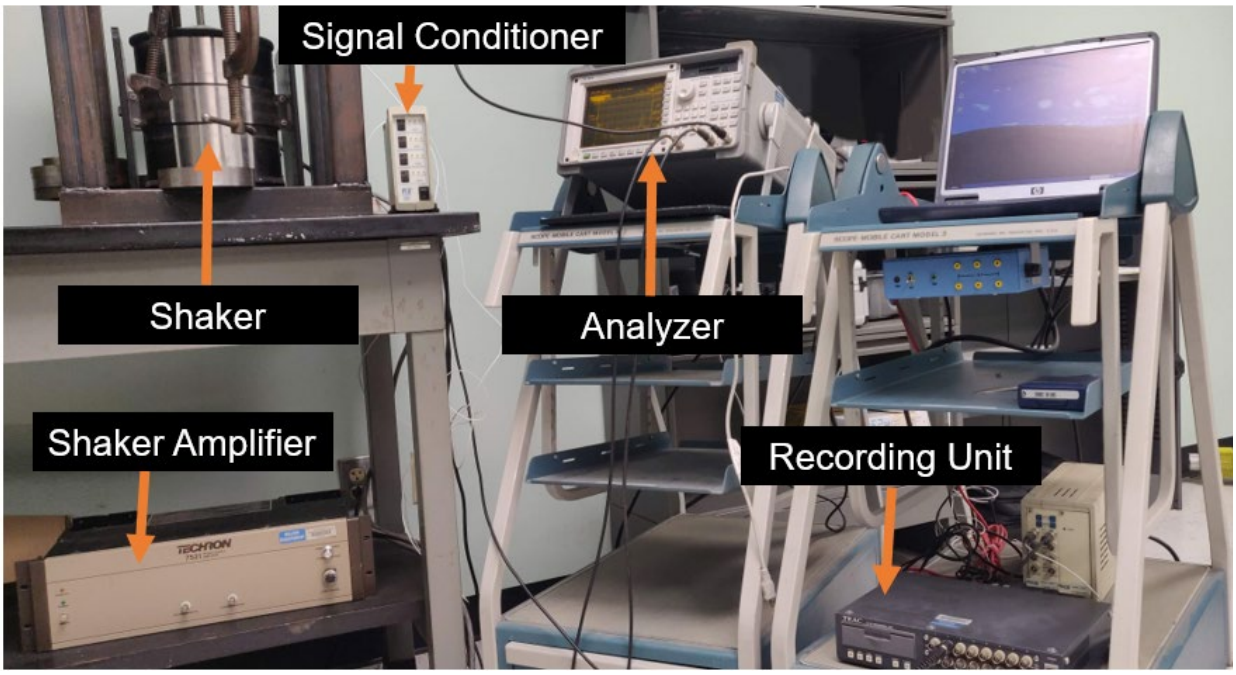

Figure 5.9: Experimental Setup

5.4 Experimental Run

The experiment run started with the determination of the volume displacement of the sensor in response to an excitation. The volume displacement was obtained by obtaining the displacement of discreet points on the sensor from the acceleration of those points recorded using an accelerometer mounted. The volume displacement was then calculated by integrating the displacement of those points and multiplying by the width of the substrate. The sensor was afterwards subjected to harmonic excitations of different frequencies as well as random excitations and the voltage from the PVDF sensor in response to those excitations were recorded. The recorded voltage data was fed through the code written based on the theoretical development of the sensor presented in chapter three of this thesis to obtain the excitation force. The calculated force and the

excitation force are compared to show the functionality and the accuracy of the sensor. These comparison results of the sensor are presented in chapter five of this thesis.

Chapter 6
Results and Discussions

6.1 Overview

This chapter presents conclusions based on the theoretical development, simulations and the experimental runs from the preceding chapters of this thesis. In this chapter, the results of the experimental run are presented in form of a comparison between the measured excitation and the applied excitation attempting to validate the objective of this research work which is to develop a force sensor for dynamic forces. Limitations of the experiment is also discussed and finally future work and improvement opportunities is presented.

6.2 Results

The developed sensor was excited by harmonic forces of different frequencies and magnitudes. The comparison between the excitation forces and the measured force by the sensor is presented here.

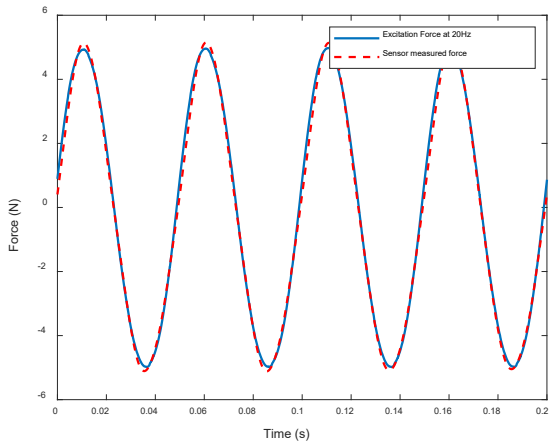

Figure 6.1: Result at 20Hz

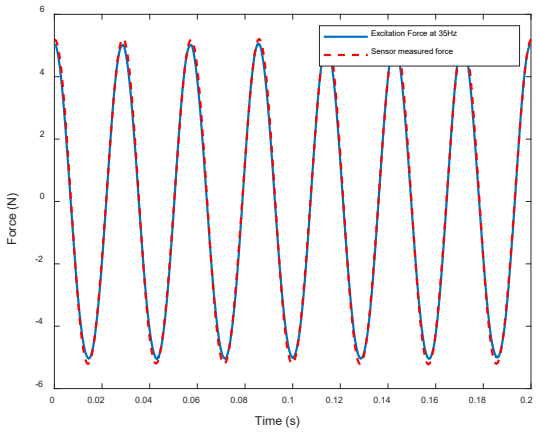

Figure 6.1b: Result at 35Hz

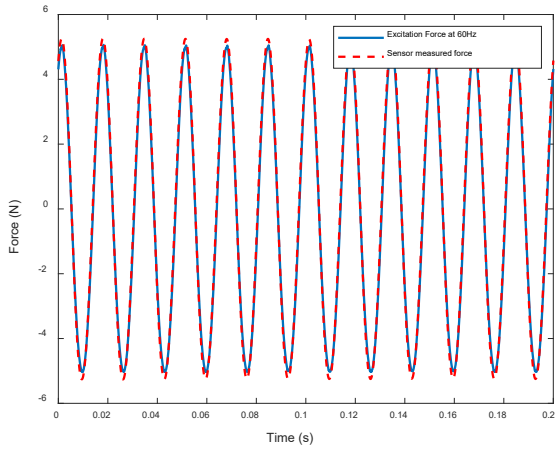

Figure 6.1c: Result at 60Hz

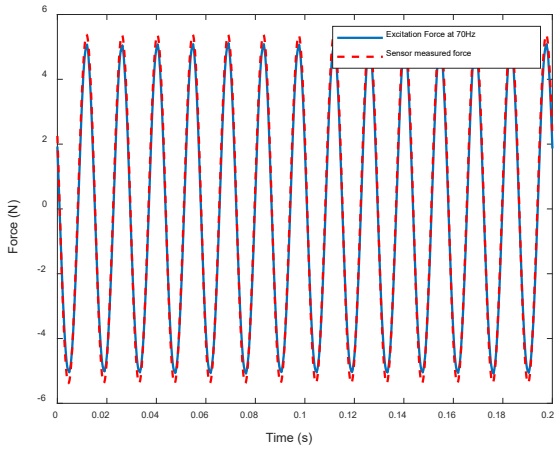

Figure 6.1d: Result at 70Hz

The sensor was also tested against random forces and obtained the result shown

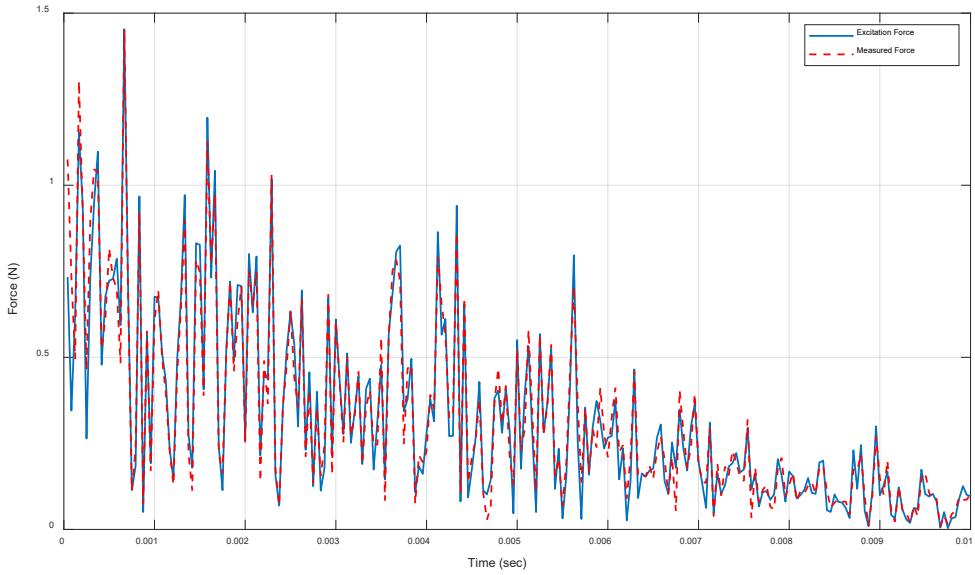

Figure 6.2: Sensor response to random excitation

The sensor error is ±7%. The results obtained for the different forms of excitation on the sensor show the accuracy as well as the measurement repeatability of forces by the sensor. The final sensor equation is given in Eqn. (6 - 1).

$$\boldsymbol{P_m} = qf(\omega)^{-1} \tag{6 – 1}$$

where

$$f(\omega) = \frac{1}{-2\omega^6 + 3.2\omega^5 + 2.5^4 - 3.2\omega^3 - 3.7\omega^2 + 5.6\omega - 9.9}$$

6.3 Temperature Change Effect on the Sensor

A PVDF film does not only have piezoelectric properties but also a pyroelectric property in which there is a generation of the electric charge in response to a significant temperature changes of the film. There is a change in temperature of material as a result of an applied strain rate. This temperature increase of the material can be obtained using Eqn. 6-2. Kapoor and Nemat-Nassar [34]

$$\Delta T = \frac{\eta}{\rho C_p} \int_0^{\epsilon} \sigma d\epsilon \tag{6 – 2}$$

where

ΔT is the change in temperature in Kelvin

η is the fraction of work done to heat the material

σ is the stress on the material and

ϵ is the strain

C_p is the specific heat capacity of the material

Using Eqn. 6-2 under the experimental condition (20^{O}C room temperature), with a force of 10N from the signal analyzer and assuming all the work done by the force is converted, Eqn. 6-2 can be evaluated as

$$\Delta T = \frac{\eta E \epsilon^2}{2\rho C_p} \qquad (6-3)$$

where

$$\epsilon = \frac{M}{ZE}$$

M = 0.287 (Bending moment of the substrate)

Z = 2x10^{-8} (Section modulus of the substrate)

E = 70GPa (Modulus of elasticity)

The temperature change using the evaluated Eqn. 6-3 is 0.6^{O}C.

From Table 4-1, the pyroelectric constant of the film as 30x10^{-6} C/m^{2}K.

The area A_f of the PVDF film is

$$A_f = 2\int_0^{0.23} A(x^2 - Lx)dx \qquad (6-4)$$

Yielding

$A_f = 0.0048\ m^2$

Hence, the Pyroelectric constant of the sensor is

$$30x10^{-6}\ C/m^2 \times A_f = 1.44x10^{-7}\ C/K$$

Using the work done on the sensor in deflection and noting that

$$1\ Volt = \frac{1\ N.m}{1\ Coulomb}$$

We obtain the voltage from the sensor as

$$\frac{(10)(8 \times 10^{-11})}{(1.44x10^{-7})(273.75)} = 2.029 \times 10^{-5} V$$

The average voltage output of the sensor for the change in temperature for the applied force is $2.029 \times 10^{-5} V$ which is negligible compared to the voltage obtained during experimentation. Hence, the temperature change during the usage of the sensor is negligible and will not affect the sensing result of the sensor.

6.4 Sensor Packaging

The principles followed in the development of this sensor are in line with the objective of this research to be able to include sensing functionality in crucial mechanical components during design. However, a package was designed for the clamped-clamped substrate adopted for this research. Fig. 6.6 shows the design sensor concept and the Fig. 6.7 shows the various parts of the package.

Figure 6.3: Designed sensor package

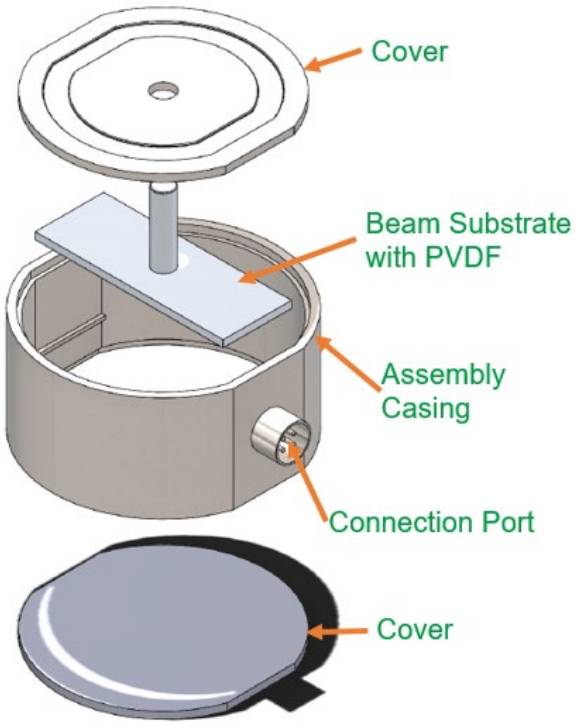

Figure 6.4: Designed sensor package

6.5 Contribution

The volume displacement approach that was adopted has been used to work on movement and deflection of membranes for sound cancellation. In this research, we employed this approach to develop the dynamic force sensor. While the local area of interest was the focus in this sound cancellation implementation, this research applied the volume displacement to the entire surface of the beam substrate of the sensor.

6.6 Conclusion

In this study, the development of a dynamic force sensor was presented and the results obtained from experiments showed the accuracy of this sensor. This shows that the sensor

development can be applied to any desired application during the design phase of a machinery by carefully choosing the substrate as well as the boundary conditions of the substrate for the effective function of the sensor.

6.7 Future Work

As it stands currently, the sensor output is obtained by the post processing of the data collected using code written in MATLAB. While this approach enabled us to show the workability of this sensor, the future work will be focused on packaging the sensor to include a signal processing electronics to ensure the real-time measurement of excitations.

APPENDICES

Appendix A: Post Processing code

```
for ii = 1:length(file_handle)
    filename = strcat("N_5/valid_volt",num2str(file_handle(ii)),'hz','.mat');
    force_data = load(filename);
    validation_data = force_data.LocalDouble;
    %
    % data rectifying around zero
    %

    high_peak_ = max(validation_data);
    low_peak_ = min(validation_data);
    span_ = high_peak_ - low_peak_;
    pt_peaks_ = span_/2;
    offset_ = high_peak_ - pt_peaks_;

    for mm = 1:length(validation_data(:,1))
        rectified_data(mm,1) = validation_data(mm,1) - offset_(1);
        rectified_data(mm,2) = validation_data(mm,2) - offset_(2);
    end

    % align the signal if out of phase
    find_delay = finddelay(rectified_data(:,2),rectified_data(:,1));
    % force measured from the PCB
    if(find_delay < 0)
        PCB_Force_volt = rectified_data(1:end-abs(find_delay),1);
        voltage = rectified_data(abs(find_delay)+1:end,2);

    elseif(find_delay > 0)
        PCB_Force_volt = rectified_data(abs(find_delay):end,1);
        voltage = rectified_data(1:(end-abs(find_delay)+1),2);

    end

     % voltage conversion to force 11241mV/kN
    s = 11.241e-3;

    PCB_Force = PCB_Force_volt/s;

     % determine the signal frequency using fft
    % sampling frequency
    data_rate = 24000;

    % sampling period T
    T = 1/data_rate;

    % length of acquired signal
    L_sig = length(PCB_Force_volt);

    % time factor t
```

```
    t = (0:L_sig-1)*T;
     % determine the signal frequency using fft
    % sampling frequency
    data_rate = 24000;

    % sampling period T
    T = 1/data_rate;

    % length of acquired signal
    L_sig = length(PCB_Force_volt);

    % time factor t
    t = (0:L_sig-1)*T;


    Y = fft(PCB_Force_volt);
    P2 = abs(Y/L_sig);
    P1 = P2(1:round(L_sig/2+1));
    P1(2:end-1) = 2*P1(2:end-1);
    f = data_rate*(0:(L_sig/2))/L_sig;
    f_Hz = round(f(find(P1==max(P1))));

    pm_index(ii) = find(PCB_Force ==max(PCB_Force),1);
    max_pcb(ii) = PCB_Force(pm_index(ii));


    f_omega(ii) = max(PCB_Force)/max(voltage);




    omega = 2*pi*file_handle(ii);


    y_cubic = [-2 3.2 2.5 -3.2 -3.7 5.6 -9.9];

    z = (omega - 2.4e2)/1.3e2;

    K = polyval(y_cubic,z);



    Pm = voltage*K;


end

clear all
```

```
% force/voltage data
force_data = load('rand/valid_voltr1.mat');
validation_data = force_data.LocalDouble;
data_length = length(validation_data(:,1));

% sampling frequency
data_rate = 24000;


% sampling period T
T = 1/data_rate;


% length of acquired signal
L = data_length;


% time factor t
t = (0:L-1)*T;


 find_delay = finddelay(validation_data(:,2),validation_data(:,1));
if(find_delay < 0)
        PCB_Force_volt = validation_data(1:end-abs(find_delay),1);
    elseif(find_delay > 0)
        PCB_Force_volt = validation_data(abs(find_delay):end,1);
end
first_force_pt = PCB_Force_volt(1);
if(first_force_pt > 0)
    temp_force = PCB_Force_volt - abs(first_force_pt);
elseif(first_force_pt < 0)
    temp_force = PCB_Force_volt + abs(first_force_pt);
end


first_volt_pt = validation_data(1,2);
if(first_volt_pt > 0)
    temp_volt = validation_data(:,2) - abs(first_volt_pt);
elseif(first_volt_pt < 0)
    temp_volt = validation_data(:,2) + abs(first_volt_pt);
end


clear temp_force
clear temp_volt


temp_force = PCB_Force_volt;
temp_volt = validation_data(:,2);
```

```
% voltage conversion to force 11241mV/kN
s = 11.241e-3;


Y = fft(temp_force);
P2 = abs(Y/L);
P1 = P2(1:round(L/2));
P1(2:end-1) = 2*P1(2:end-1);
f = data_rate*(0:floor(L/2))/L;
omega = 2*pi*f;

Y2 = fft(temp_volt);
P22 = abs(Y2/L);
P12 = P22(1:round(L/2));
P12(2:end-1) = 2*P12(2:end-1);
f2 = data_rate*(0:floor(L/2))/L;
omega2 = 2*pi*f2;


for ii = 2:length(omega)

    y_cubic = [-2 3.2 2.5 -3.2 -3.7 5.6 -9.9];

    z(ii) = (omega(ii) - 2.4e2)/1.3e2;

    K(ii) = polyval(y_cubic,z(ii));


    Pm(ii) = P12(ii)*K(ii);

%     predicted(ii) = CONST*P12(ii)*freq_diff(ii);

end
```

References

[1] R. S. Dahiya, M. Valle, (2013) Robotic Tactile Sensing. Springer. 2013

[2] Grzybek D. 1995, Piezoelectric generators: material and structures. Pomiary Automatyka Robotyka nr 10/2013

[3] Wedlock B.D, (1964) Properties of Piezoelectric materials. U.S. Army Materials Research Agency

[4] Furukawa T. (1989) Piezoelectricity and Pyroelectricity in Polymers. IEEE Transactions on Electrical insulation Vol. 24 No.3

[5] Boris Gusarov. PVDF piezoelectric polymers: characterization and application to thermal energy harvesting. Electric power. Université Grenoble Alpes, 2015. English. NNT : 2015GREAT091

[6] Katzir S. (2003) The Discovery of the Piezoelectric Effect. Arch. Hist. Exact Sci 57 (2003) 61 – 91

[7] Alfredo V (2000) Novel Piezoelectric transducers for high voltage measurements. Universitat Politecnica de catalunya

[8] Patrick T Summers, Yanyun Chen, Christian M Rippe, Ben Allen, Adrian P Mouritz, Scott W Case, Brian Y Lattimer (2015) Overview of aluminum alloy mechanical properties during and after fires.

[9] D Faust, R Lakes (2015) Temperature and Substrate Dependence of Piezoelectric Sensitivity for PVDF Films. Ferroelectrics Volume 481

[10] ANSI/IEEE, IEEE standard on piezoelectricity. IEEE Standard 176-1987 (1987)

[11] Jaakko Palosaari, Energy Harvesting from walking using piezoelectric cymbal and diaphragm type structures. (2017) Acta univ. Oul. c630

[12] Michael Friswell, Sondipon Adhikari (2010) Sensor shape design for piezoelectric cantilever beams to harvest vibration energy. Journal of Applied physics 108, 014901

[13] Y. Kamata, D. Yoon, T. Sasaki, Y. Nozaki, S. Yamaura, (2016) Development of a Simple Fabrication Process for a printable Piezoelectric Enegy Harvest Device. IEEE 11th Annual international conference on Nano/Micro Engineered and Molecular systems 2016 page 520 - 523

[14] B.L.F. Daku, E.M.A. Mohamed, A.F. Prugger (2004) A PVDF transducer for low-frequency acceleration measurements. ISA transactions 43. 319-328

[15] J. Sirohi, I. Chopra (2001) Fundamental understanding of piezoelectric strain sensors. Journal of intelligent material systems and structures, vol 11

[16] Piezo Film Sensors technical manual, (1999) Measurement Specialties Inc. P/N 1005663-1 REV B

[17] M.B. Zahui, J.W. Kamman, K. Naghshineh (2001) Theoretical Development and Experimental Validation of Local Volume DIsplacement sensor for a vibrating Beam. ASME Vol. 123

[19] Freitas, V.F., Santos, I.A., Botero, É., Fraygola, B.M., Garcia, D. and Eiras, J.A. (2011), Piezoelectric Characterization of (0.6)BiFeO3–(0.4)PbTiO3 Multiferroic Ceramics.

Journal of the American Ceramic Society, 94: 754-758. doi:10.1111/j.1551-2916.2010.04118.x

[20] A. Kuoni, et al. "Polyimide membrane with ZnO piezoelectric thin film pressure transducers as a differential pressure liquid flow sensor." Journal of Micromechanics and Microengineering 13.4 (2003): S103

[21] Allan G. Piersol, (2002) Harris' Shock and Vibration Handbook. McGraw-Hill

[22] https://instrumentationandcontrollers.blogspot.com/2010/11/load-cell-and-load-cell-types.html viewed on 7/1/2020

[23] https://www.avnet.com/wps/portal/abacus/solutions/technologies/sensors/pressure-sensors/core-technologies/piezoelectric/ viewed on 7/1/2020

[24] M.A K. P. Tolentino, D. R. B. Albano, F. B. Sevilla,Piezoelectric sensor for ethylene based on silver(I)/polymer composite,Sensors and Actuators B: Chemical,Volume 254,2018,Pages 299-306,ISSN 0925-4005,

[25] Di Rito, G.; Chiarelli, M.R.; Luciano, B. Dynamic Modelling and Experimental Characterization of a Self-Powered Structural Health-Monitoring System with MFC Piezoelectric Patches. Sensors 2020, 20, 950

[26] Tarhini, H., Itani, R., Fakih, M. A., & Mustapha, S. (2018). Optimization of piezoelectric wafer placement for structural health-monitoring applications. Journal of Intelligent Material Systems and Structures, 29(19), 3758–3773

[27] Bela, L (2003) Instrument engineer' handbook: Process measurement and analysis. CRC Press.

[28] https://www.gabrian.com/wp-content/uploads/2018/09/6061-Aluminum-Alloy-Properties-1.pdf viewed on 7/21/2020

[29] Johnson M.E., Elliott S.J. 1995, Active Control of Sound Radiation Using volume velocity cancellation. Journal of the Acoustic Society of America, 98(4), pp. 2174-2186

[30] Pietrzko S., Mao Q. 2009, Design of Volume Displacement Sensor. Mechanics. Vol. 28 No. 2 2009

[31] Lee C.K., Moon F.C. (1990) Modal Sensors/Actuators. Journal of Applied Mechanics. Vol. 112

[32] Fraden J. (2010) Handbook of modern Sensors. Fourth edition. Springer

[33] Rao S. (2011) Mechanical vibrations. Fifth Edition. Prentice Hall

[34] Kapoor R and Nemat-Nasser S (1998) Determination of temperature rise during high strain rate deformation. Mechanics of Materials 27 1-12